DE-FG05-80ET-53088-699 IFSR #699

Area Preserving Nontwist Maps: Periodic Orbits and Transition to Chaos

D. DEL CASTILLO NEGRETE,[a] J.M. GREENE,[b] and P.J. MORRISON
Department of Physics and Institute for Fusion Studies
The University of Texas at Austin
Austin, Texas 78712

March 1995

[a] Present address: Scripps Institution of Oceanography,
University of California at San Diego, La Jolla, CA 92093-0230
[b] General Atomics Inc., San Diego, CA 92186-9784

Area Preserving Nontwist Maps: Periodic Orbits and Transition to Chaos

D. del-Castillo-Negrete,* J. M. Greene,† and P. J. Morrison

Department of Physics and Institute for Fusion Studies

The University of Texas at Austin, Austin, Texas 78712

March 1, 1995

Abstract

Area preserving nontwist maps, i.e. maps that violate the twist condition, are considered. A representative example, the *standard nontwist map* that violates the twist condition along a curve called the shearless curve, is studied in detail. Using symmetry lines and involutions, periodic orbits are computed and two bifurcations analyzed: periodic orbit collision and separatrix reconnection. The transition to chaos due to the destruction of the shearless curve is studied. This problem is outside the applicability of the KAM (Kolmogorov-Arnold-Moser) theorem. Using the residue criterion we compute the critical parameter values for the destruction of the shearless curve with rotation number equal to the inverse golden mean. The results indicate that the destruction of this curve is fundamentally different from the destruction of the inverse golden mean curve in twist maps. It is shown that the residues converge to a six-cycle at criticality.

KEY WORDS: area preserving map, twist, degenerate Hamiltonian, KAM curve, bifurcation.

*Present address: Scripps Institution of Oceanography, University of California at San Diego, La Jolla, CA 92093–0230.

†General Atomics Inc., San Diego, CA 92186–9784.

1 Introduction

In this paper we consider a special class of area preserving maps, M, of a two-dimensional domain onto itself. Such maps will be represented as $\mathbf{x}_{i+1} = M(\mathbf{x}_i)$, where $\mathbf{x}_i = (x_i, y_i)$ denotes a point in the domain at the i-th iteration of the map. To be area preserving, the Jacobian of the transformation from $\mathbf{x}_i$ to $\mathbf{x}_{i+1}$ must equal unity. The special class of area preserving maps of interest here violate the so-called twist condition, which will be described presently. These maps arise naturally in the study of Hamiltonian systems, and also in the study of transport problems in plasma physics, fluid dynamics, and other areas.

A large class of area preserving maps can be cast in the form,

$$x_{i+1} = x_i + \Omega(y_{i+1}) + f(x_i, y_{i+1})$$

$$y_{i+1} = y_i + g(x_i, y_{i+1})\,, \tag{1}$$

where the area preservation condition is $\partial f/\partial x_i + \partial g/\partial y_{i+1} = 0$. This form is often encountered in applications and is particularly suited for addressing a problem of paramount importance in Hamiltonian dynamics: the study of the behavior of an integrable Hamiltonian system with Hamiltonian, H_0, under the affect of a nonintegrable perturbation. The Hamiltonian of this problem has the form,

$$H = H_0(J) + H_1(\theta, J, t)\,, \tag{2}$$

where (θ, J) are the angle-action variables associated with H_0 and where H_1 describes the perturbation, which is assumed to be periodic in θ and t. It is well-known that maps of the form of Eq. (1) embody the essential features of Hamiltonian systems of the form of Eq. (2). Because of this and the fact that maps are simpler, they have been the subject of much study. The association between the two is made by identifying the map variables x

and y with the angle-action variables θ and J, respectively, and identifying the index i with intervals of t separated by the periodicity time interval of H_1.

Further, the map function Ω is identified with the frequency of the unperturbed Hamiltonian, $\partial H_0/\partial J$, and f and g represent the perturbation H_1 (e.g. [1]). A considerable amount of work, both analytical and numerical, has been devoted to the study of maps of the form of Eq. (1) (e.g. [2, 3]); however, most studies have been restricted to maps that satisfy the *twist condition*,

$$\frac{\partial \Omega}{\partial y_{i+1}} \neq 0\,, \tag{3}$$

which is the map analogue of the *nondegeneracy condition* for Hamiltonian systems,

$$\frac{\partial^2 H_0}{\partial J^2} \neq 0\,. \tag{4}$$

Here, a map that violates Eq. (3) will be called a *nontwist map* (which should not be confused with a no-twist map which satisfies $\partial\Omega/\partial y_{i+1} \equiv 0$).

One of the main reasons why the twist condition is assumed in most studies is because it arises naturally in classical Hamiltonian particle mechanics. Also, the twist condition is a crucial assumption in the proofs of several important theorems, including the celebrated KAM (Kolmogorov-Arnold-Moser) theorem [4]. At present, no analogue of the KAM theorem for nontwist maps exists. In addition to its mathematical significance, the study of degenerate Hamiltonians and nontwist maps is important because, as will be detailed below, such systems naturally occur in a variety of problems of plasma physics, fluid dynamics, celestial mechanics, and other areas.

One of the simplest area preserving nontwist maps is

$$x_{n+1} = x_n + a(1 - y_{n+1}^p) \tag{5}$$

$$y_{n+1} = y_n - b\,\sin\left(2\pi x_n\right), \tag{6}$$

where, a and b are real numbers, $p > 1$ is a positive integer, and the domain of interest is

$D := \{(x,y) \,|\, y \in (-\infty,\infty) \text{ and } x \in (-1/2,1/2) \bmod 1\}$. Equation (5) can be viewed as the first two terms in the Taylor expansion of the function Ω about the point where the twist condition fails; thus it describes the behavior near such a point in a general map. In the present paper, we restrict attention to the special case where $p = 2$, and, following the terminology of [5], we call the resulting map the *standard nontwist map.* Some aspects of this map have been previously studied by [6, 7, 5, 8, 9].

For $b = 0$ the standard nontwist map is integrable—successive iterations of initial conditions lie on straight lines that wrap around the x-domain. Orbits for which the rotation number (cf. Eq. (7) below) is irrational are called invariant circles or KAM curves. Under the effect of the perturbation, some KAM curves are destroyed whereas others persist. The study of the destruction of KAM curves is of importance in many applications since, in a two-dimensional phase space, KAM curves are barriers to transport and their breakup signals the lack of confinement. In the $b = 0$ limit, we call the $y = 0$ line the *shearless curve* because along it the shear, $\partial x_{n+1}/\partial y_{n+1}$, vanishes. The rotation number (Eq. (7)) of the shearless curve depends on the parameters a and b, and there are curves in the (a,b)-plane corresponding to constant shearless rotation number; these curves are called bifurcation curves and will be discussed in Sec. 2.2. As the values of a and b change the shearless curve bends and eventually breaks. One of the objectives of this paper is to understand when and how this happens; this is the problem we call the *transition to chaos in nontwist maps.* In particular, we compute the (a,b) critical parameter values for which the shearless curve with the rotation number equal to the inverse golden mean, $1/\gamma := (\sqrt{5}-1)/2$, is destroyed. Since the twist condition fails along the shearless curve, this problem is outside the range of applicability of KAM theory. The numerical results presented here show that, due to the violation of the twist condition, the destruction of the $1/\gamma$ shearless curve is fundamentally different from the destruction of the $1/\gamma$ KAM curve in twist maps, such as the standard map.

The study of the transition to chaos presented here relies upon the use of periodic orbits to determine the existence of KAM curves. It is for this reason that we first discuss periodic orbits in the standard nontwist map. However, independently of its use in the study of KAM curves, the study of periodic orbits in nontwist maps is interesting in its own right. The violation of the twist condition gives rise to a rich variety of bifurcations. We discuss two of them: periodic orbit collision and separatrix reconnection. Periodic orbit collision is a bifurcation that takes place when periodic orbits on each side of the shearless curve approach each other, merge at the shearless curve, and eventually annihilate. Understanding this bifurcation is crucial when using periodic orbits to study KAM curves. The other bifurcation studied, separatrix reconnection, is a global bifurcation of the phase space topology in the vicinity of the shearless curve. Some aspects of this bifurcation have been studied in [6, 10, 5, 8, 9]. Here, we propose a general criterion for determining the separatrix reconnection threshold in the standard nontwist map.

The breakup of KAM curves in area preserving maps exhibits universal critical scaling behavior [12, 13]. This means that there is a state, called the critical state, in which the system is scale invariant and that this property depends only on very general features. The renormalization group method is a general technique for studying systems of this type. In a way akin to what is done in the theory of phase transitions, universality classes can be introduced for classifying the fundamentally different ways in which a KAM curve can be destroyed. In a future publication [14], we study the critical behavior of the shearless curve in the standard nontwist map by using the renormalization group formalism for area preserving maps [15, 16, 17]. In particular, we show that the scaling properties of the $1/\gamma$ shearless curve at criticality are different from the scaling properties of the $1/\gamma$ KAM curve in twist maps. Also, it is shown that the standard nontwist map at the threshold parameter values for the destruction of the shearless curve is on the stable manifold of a period-twelve fixed point of the renormalization operator. This period-twelve fixed point defines a new universality

class for the destruction of the inverse golden mean KAM curve, the one corresponding to nontwist maps. Moreover, it is shown that the period-twelve fixed point has at least two unstable eigenvalues.

Since nontwist maps have not hitherto been studied in great detail, we describe now some of the applications of such maps. Recently, the problem of passive advection in two-dimensional incompressible flows has gained attention in the fluid dynamics community. Part of the appeal of this problem is that it can be formulated as a Hamiltonian dynamics problem with the streamfunction playing the role of the Hamiltonian (e.g. [18] and references therein). Hence, one can use methods of Hamiltonian chaos theory for studying transport and mixing in fluids. An application of this approach is the study of transport by traveling waves in shear flow. This problem is of interest in geophysical fluid dynamics, where wave propagation in strong global shear flows, which are know generically as "jets" or "zonal flows," is an ubiquitous phenomena. In [19, 5, 20] it was shown that all shear flows with nonmonotonic velocity profiles give rise to degenerate Hamiltonian systems and therefore to maps that violate the twist condition. Experimentally it has been observed [21], and in simplified models shown [5], that nonmonotonic shear flows possess a strong transport barrier that is located in the region where the velocity profile attains its maximum. Understanding when and how this transport barrier breaks is an important problem. In the standard nontwist map model [5], the shearless curve corresponds to the barrier, and the problem of transition to chaos corresponds to the problem of global transport due to the destruction of the barrier. Other work on the application of nontwist maps to fluid transport problems is that of [7], where the traveling wave map (which corresponds to the standard nontwist map with $a = b$) was used to study diffusion by traveling waves, and that of [22], where a modification of the traveling wave map was used to study mixing in terms of finite-time Liapunov exponents.

An important application of area preserving maps, and historically one of the earliest, is to

the study of magnetic field lines in toroidal plasma devices, such as tokamaks and stellarators (e.g. [23] and references therein). In the equilibrium configurations of such devices, magnetic field lines lie on and wrap helically around nested tori. The average pitch (rotation number) of this wrapping is described by the "q-profile," and monotonicity of the q-profile amounts to the twist condition of the associated maps. Under usual conditions the q-profile is monotonic; however, there are important situations in which it is not. For example, nonmonotonic q-profiles can occur during the early stage of tokamak discharges if the current rise is sufficiently fast. An understanding of the magnetic field in such a situation might shed some light on the experimentally observed anomalously fast current penetration [24]. The standard nontwist map provides a simple model for studying magnetic field line stochasticity and reconnection in nonmonotonic q-profiles [19]. A remarkable feature of the standard nontwist map is the robustness of the shearless curve (cf. Fig. 13), which suggests that a reduction of the magnetic field shear could be directly related to higher confinement. Some experimental evidence for this exists [25].

Another area where nontwist maps play a role is in the study of $\mathbf{E} \times \mathbf{B}$ transport in magnetized plasma. The $\mathbf{E} \times \mathbf{B}$ drift equations of motion are Hamiltonian with the electrostatic potential being the Hamiltonian [27]. Accordingly, transport in the plane perpendicular to the magnetic field can be modeled with an area preserving map, one which will violate the twist condition if the radial electric field is not monotonic. Nonmonotonic radial electric fields are believed to be present in the tokamak edge during the high confinement (H-mode) regime [26].

Nontwist maps also arise in celestial mechanics. Planetary potentials are not exactly spherically symmetric, in particular, the oblateness of the planets introduces corrections to the Keplerian orbits. The effect of these corrections can be analyzed by studying the dynamics of a particle in a general axisymmetric gravitational potential. This problem can be reduced to a one and a half degree-of-freedom Hamiltonian system, from which an

area preserving map can be constructed [28]. The map so derived possesses two interesting features: first, for a specific inclination (known as the critical inclination) of the particle orbit, the twist vanishes, i.e. $\Omega = 0$ (cf. Eq. (1)) and second, for a different orbit inclination, the shear vanishes, i.e. $d\Omega/dy = 0$, and therefore the map is a nontwist map. Understanding the implications of the violation of the twist condition on the particles trajectories is an interesting problem.

Degenerate Hamiltonians have also been studied by Zaslavsky, Sagdeev and collaborators (e.g. [29] and references therein). However, there are some important distinctions between their work and the work presented here. These authors have studied nonlinear perturbations of linear Hamiltonians. Hamiltonians of this type appear, for example, when studying the motion of a particle in a constant magnetic field and the field of a plane wave traveling perpendicularly to the magnetic field. Since linear Hamiltonians (i.e. ones for which $H_0(J) \propto J$) are degenerate for all values of the action, degeneracy in these systems is *global* whereas in the systems studied in the present paper the degeneracy is *local* (i.e. Eq. (4) is violated only for a specific value of the action J). When a specific resonance condition is met, global degeneracy gives rise to the so-called stochastic web which exhibits an interesting and rich dynamics [29]. However, globally degenerate Hamiltonians are not structurally stable: the presence of a nonlinearity in the unperturbed Hamiltonian and a small resonance detuning (both to be expected in physical applications) will render the global degeneracy local. Locally degenerate Hamiltonians are, on the other hand, structurally stable. In addition to the issue of structural stability, locally degenerate Hamiltonians are better suited for the study of the breakdown of KAM theory because in these systems the degeneracy is localized and the destruction of KAM curves in the region of degeneracy can be isolated. In globally degenerate Hamiltonians, the destruction of KAM curves is hard to isolate; as soon as the perturbation is present, all the unperturbed KAM curves are destroyed due to changes in the phase space topology.

Another relevant application is the recent work of [30], where it is shown that the dynamics of a particle in a cylindrically symmetric potential well, subjected to time-periodic radial kicks, can be reduced to a degenerate Hamiltonian system, from which a nontwist map can be constructed. The author shows that this problem is equivalent to that of the dynamics of rays in a cylindrical waveguide with a periodic array of lenses along its axis. Other uses of nontwist maps, include work on particle accelerators [31] and plasma wave heating [32].

The paper is organized as follows: Section 2 contains a study of periodic orbits in the standard nontwist map. First it is shown how these orbits can be computed with the aid of symmetry lines and involutions. Following this, we discuss periodic orbit collisions and bifurcation curves. Sec. 3 is devoted to a study of separatrix reconnection. The reconnection thresholds for period-one and period-two orbits in the standard nontwist map are computed, and a general method for computing the reconnection threshold of period-n ($n > 2$) is presented. In Sec. 4 we address the transition to chaos in the standard nontwist map. The shearless curve is defined using the periodic orbit approximation and the critical parameter values, (a_c, b_c), for its destruction are found using the residue criterion. The results presented in the present paper are based on [8]. In a forthcoming publication [14] we present a renormalization group study of the transition to chaos in nontwist maps.

2 Periodic Orbits

A point $\mathbf{x}$ generates a *periodic orbit* of *order* n if $M^n\mathbf{x} = \mathbf{x}$. The *rotation number* associated with a periodic orbit is the rational number m/n, where n is the order of the periodic orbit and m is the integer number of times the orbit cycles through the x-domain before returning to its initial position. In general, the rotation number ω of an orbit generated by a point (x, y) is defined, when it exists, by the limit

$$\omega := \lim_{n\to\infty} \frac{x_n}{n}, \tag{7}$$

where, in this definition, the x-coordinate is lifted to the entire real line (i.e. x_n is not taken modulo 1).

Periodic orbits comprise a template that guides the study of Hamiltonian systems, in particular, one that is useful for studying the destruction of KAM curves. In this section we discuss periodic orbits of the standard nontwist map. We begin by showing how these orbits can be computed using symmetry lines and involutions, and then we discuss periodic orbit collisions and bifurcation curves.

2.1 Symmetry lines and involutions

The numerical search for periodic orbits is in general a difficult two-dimensional root finding problem. However, the use of symmetries reduces this to one-dimension, thereby making the problem tractable [33, 11]. Discrete symmetries of Hamiltonian systems, unlike continuous symmetries, do not give rise to integrals of motion. However, they are of value for organizing and finding periodic orbits. A transformation T is called a *symmetry* of a map M if

$$M = T^{-1}MT\,, \tag{8}$$

that is, if the map remains invariant under T. For example, it can easily be checked that the standard nontwist map has the following symmetry:

$$T(x,y) = (x + 1/2, -y)\,. \tag{9}$$

This symmetry will be useful for organizing the periodic orbits.

A transformation I_0 will be called a *time reversal symmetry* if

$$M^{-1} = I_0^{-1}MI_0\,. \tag{10}$$

That is, applying a time reversal symmetry to a map is equivalent to running the map backwards in time. An example of a time reversal symmetry in a time continuous Hamiltonian system is the transformation $p \to -p$, which in a Hamiltonian of the standard form

$H = p^2/2m + V(q)$, is equivalent to time reversal, $t \to -t$. If the time reversal symmetry I_0 is an *involution*, that is, if

$$I_0^2 = 1\,, \tag{11}$$

then it can be used to construct another time reversal symmetry of M:

$$I_1 := MI_0 \tag{12}$$

which is also an involution. With the aid of the involutions I_0 and I_1, the map M can be factored as

$$M = I_1 I_0\,. \tag{13}$$

In general, maps that can be factored as a product of involutions are called *reversible* maps [34, 33]. The standard nontwist map has the following time reversal symmetry

$$I_0(x, y) = (-x, y - b\sin(2\pi x))\ , \tag{14}$$

which is easy to show is an involution and, according to Eq. (12), can be used to generate the second time reversal symmetry,

$$I_1(x, y) = \left(-x + a(1 - y^2), y\right)\ . \tag{15}$$

Thus, using Eq. (14) and Eq. (15), the standard nontwist map can be factored as Eq. (13).

The invariant sets of the involution maps,

$$\mathcal{I}_{0,1} = \{\mathbf{x} \mid I_{0,1}\mathbf{x} = \mathbf{x}\}\,, \tag{16}$$

are one-dimensional sets called the *symmetry sets* of the map. Once the sets $\mathcal{I}_{0,1}$ are known, the search for periodic orbits can be reduced to a one-dimensional root finding problem using the following result:

If $\mathbf{x} \in \mathcal{I}_{0,1}$ then

$$M^n\mathbf{x} = \mathbf{x} \text{ if and only if } \begin{cases} M^{n/2}\,\mathbf{x} \in \mathcal{I}_{0,1} & \text{for } n \text{ even} \\ M^{(n\pm1)/2}\,\mathbf{x} \in \mathcal{I}_{1,0} & \text{for } n \text{ odd}\,. \end{cases} \tag{17}$$

That is, according to this result, periodic orbits can be found by searching in the one-dimensional sets $\mathcal{I}_{0,1}$, rather than in the whole domain. To prove this result for the case when n is even, let $\mathbf{x} \in \mathcal{I}_{0,1}$ and suppose that $M^n\mathbf{x} = \mathbf{x}$. Then

$$I_{0,1}M^{n/2}\mathbf{x} = I_{0,1}M^{-n/2}\mathbf{x} = I_{0,1}M^{-n/2}I_{0,1}\mathbf{x} = M^{n/2}\mathbf{x}\,, \tag{18}$$

and therefore $M^{n/2}\mathbf{x} \in \mathcal{I}_{0,1}$. The first equality of Eq. (18) follows from $M^n\mathbf{x} = \mathbf{x}$, the second from $I_{0,1}\mathbf{x} = \mathbf{x}$, while the third requires writing out the involution decomposition of M. Conversely, assume $M^{n/2}\mathbf{x} \in \mathcal{I}_{0,1}$, then

$$M^n\mathbf{x} = M^{n/2}I_{0,1}I_{0,1}M^{n/2}\mathbf{x} = M^{n/2}I_{0,1}M^{n/2}\mathbf{x} = I_{0,1}\mathbf{x} = \mathbf{x}\,,$$

which establishes half of Eq. (17). The proof for the case when n is odd is similar. In general, the j-th involution is defined as $I_j := M^jI_0$ and its invariant sets are higher order symmetry sets $\mathcal{I}_j := \{\mathbf{x}|I_j\mathbf{x} = \mathbf{x}\}$. Periodic orbits of different orders can then be found at the intersection of these sets; for example, if $\mathbf{x} \in \mathcal{I}_j \bigcap \mathcal{I}_k$, then $M^{j-k}\mathbf{x} = \mathbf{x}$.

The symmetry sets $\mathcal{I}_{0,1} = \{\mathbf{x}|I_{0,1}\mathbf{x} = \mathbf{x}\}$ for the standard nontwist map are depicted in Fig. 1. The set $\mathcal{I}_0$ is the union of the following *symmetry lines*:

$$s_1 = \{(x,y) \mid x = 0\}\,, \qquad s_2 = \{(x,y) \mid x = 1/2\}\,, \tag{19}$$

while the invariant set $\mathcal{I}_1$ is the union of

$$s_3 = \{(x,y) \mid x = a(1-y^2)/2\}\,, \quad s_4 = \{(x,y) \mid x = a(1-y^2)/2 + 1/2\}\,. \tag{20}$$

Given the symmetry lines, periodic orbits can be found relatively easily using Eq. (17). For example, periodic orbits with n odd on the s_1 symmetry line are obtained by looking for points $\mathbf{x} = (0,y)$ on s_1 that are mapped to s_3 or s_4 after $(n+1)/2$ iterations. This is implemented as a one-dimensional root finding problem by seeking the zeros of the function $F(y) = \sin\left[2\pi\left(\widehat{x} - a(1-\widehat{y}^2)/2\right)\right] = 0$, where $\widehat{x}$ and $\widehat{y}$ are functions of y via

$(\widehat{x},\widehat{y}) := M^{(n+1)/2}(0,y)$. The sine function in $F(y)$ is included to remove the distinction between s_3 and s_4; however, it is a simple matter to ascertain this after the periodic orbit is found. Similar ideas are applied to find other periodic orbits.

Periodic orbits follow a *routing pattern*, i.e. a visitation sequence to the various symmetry lines. In particular, a periodic orbit with rotation number m/n that starts on a symmetry line s_i is mapped to another symmetry line s_j after $q < n$ iterations, according to the following routing pattern:

$$\text{If} \quad m/n = \begin{cases} \text{odd/even} \\ \text{odd/odd} \\ \text{even/odd} \end{cases}, \quad \text{then} \quad \begin{cases} s_1 \rightleftharpoons s_2 \\ s_3 \rightleftharpoons s_4 \end{cases} \text{ or } \begin{cases} s_1 \rightleftharpoons s_4 \\ s_2 \rightleftharpoons s_3 \end{cases} \text{ or } \begin{cases} s_1 \rightleftharpoons s_3 \\ s_2 \rightleftharpoons s_4 \end{cases}, \tag{21}$$

where $s_i \rightleftharpoons s_j$ means that a point on s_i (s_j) is mapped to s_j (s_i) after $n/2$ iterations when n is even, or after $(n+1)/2$ iterations when n is odd. See for example, Fig. 1, where the circles and crosses represent periodic orbits with $m/n = 1/3$.

Because of the violation of the twist condition, periodic orbits in the standard nontwist map come in pairs; contrary to what happens typically in twist maps, there are two periodic orbits with the *same* rotation number on each symmetry line. This is clearly evident in the limit $b = 0$, for which periodic orbits with rotation number m/n on s_1, for example, are given by $(0, \pm\sqrt{1-(m/n)/a})$. We call the periodic orbit with the larger y-coordinate the "up" orbit and that with the smaller y-coordinate the "down" orbit (cf. Fig. 1). The up and down periodic orbits on the symmetry lines can be related by the symmetry of Eq. (9). If u_i and d_i denote, respectively, the coordinates of the up and down periodic orbits on the

symmetry line s_i, then

$$d_2 = T(u_1) \quad u_2 = T(d_1)$$
$$d_4 = T(u_3) \quad u_4 = T(d_3)\,. \tag{22}$$

Therefore, it is enough to compute periodic orbits on s_1 and s_3.

2.2 Periodic orbit collisions—bifurcation curves

In this subsection we study periodic orbit collision, a bifurcation that takes place when the up and down periodic orbits on a symmetry line meet as the standard nontwist map parameters are varied.

As said before, when $b = 0$, there are two periodic orbits with the same rotation number m/n on the symmetry line s_1. To study the behavior of these orbits as we depart from $b = 0$, we have plotted in Fig. 2 the y-coordinate of the $m/n = 3/5$ periodic orbit on s_1 as a function of b for fixed $a = 0.618$. As expected, at $b = 0$ there are two periodic orbits with $y = \pm\sqrt{1 - (3/5)/a}$. As the value of b increases, the up and down orbits approach each other and, at the bifurcation value $b = 0.44$, they collide and annihilate. For higher values of b the 3/5 orbits no longer exist in s_1. The bifurcation value of b depends on both a and m/n.

The outcome of the periodic orbits collision is closely related to the stability properties of these orbits. The stability of a periodic orbit is determined by the value of its residue [11], R, which is defined as $R := \frac{1}{4}[2 - Tr(L)]$, where L is the map M^n linearized about the periodic orbit of interest and Tr denotes the trace. If $0 < R < 1$ the orbit is stable, or elliptic; if $R < 0$ or $R > 1$ it is unstable or hyperbolic; and in the degenerate cases $R = 0$ and $R = 1$, it is parabolic. In Fig. 3 we have plotted the residues of periodic orbits on s_1, with $m/n = 3/5$, 8/13 and 21/34, as functions of a for fixed $b = 0.7425$. These plots illustrate the following generic properties of the residues. (a) At the bifurcation point the residues of the up and down orbits are zero. (b) Close to the bifurcation point, periodic orbits with n odd (even) have different (the same) stability type. (c) For m/n of the form odd/even, the

up and down residues are equal. The residues exhibit an interesting dependence on the map parameters which remains to be explored. For example, in Fig. 3(b) a sort of interchange of instability is taking place between the up and down periodic orbits. Also, as shown in Fig. 3(c), some periodic orbits exhibit a kind of stability recurrence.

To illustrate periodic orbit collision behavior, we have plotted in Fig. 9 the evolution in phase space of the 3/5 periodic orbits, with fixed $a = 0.618$ as b increases. Case (d) depicts the collision point where the elliptic and hyperbolic orbits annihilate. The topology changes shown in the intermediate stages will be discussed in the next section. The behavior of all m/n periodic orbits with odd n is qualitatively the same as that of the 3/5 orbit discussed here. Consider now periodic orbits with even n. In this case, contrary to the odd case, the up and down orbits on a given symmetry line always have the same stability type, i.e. both are elliptic or both are hyperbolic. Figure 7 depicts the evolution in phase space of the 1/4 periodic orbits, with fixed $a = 0.2625$ as b increases. This is the generic scenario for the case when n is even (except for the case $n = 2$, where the elliptic orbits never collide). Note that, when n is even the collision/annihilation process has two stages: during the first stage, cases (b) and (c) of Fig. 7, the hyperbolic orbits collide and "scatter" in a direction transverse to the symmetry line while the elliptic orbits form a "dipole." In the second stage, case (d) of Fig. 7, the two elliptic orbits forming each dipole annihilate, together with the two adjacent hyperbolic orbits.

Although these bifurcation pictures are visually pleasing, their existence is problematic when one is using periodic orbits to approximate KAM curves. The main difficulty is that, in general, it is not known a priori which periodic orbits have collided and which have annihilated. To overcome this problem we construct in the (a, b) space bifurcation curves. For a given r/s, the *r/s-bifurcation curve* is the locus of points (a, b), for which the r/s periodic orbits are at the point of collision. For the case when n is odd this corresponds to the hyperbolic-elliptic collision, e.g. Fig. 9 (d), and for the case when n is even this corresponds

to the hyperbolic-hyperbolic collision, e.g. Fig. 7 (b). In all the cases considered here, the bifurcation curves are graphs (cf. Fig. 4), which we denote by $b = \Phi_{r/s}(a)$. One of the main features of bifurcation curves is that for (a, b) values below the curve $b = \Phi_{r/s}(a)$, the r/s periodic orbits are below the collision point and hence will exist. Also, by construction, for (a, b) values on $\Phi_{r/s}$, the rotation number of the shearless curve is r/s. That is, the bifurcation curves are the locus of points in (a, b) space for which the shearless curve has constant rotation number.

3 Separatrix Reconnection

The objective of this section is to discuss separatrix reconnection in the standard nontwist map. This is a global bifurcation that changes the phase space topology in the vicinity of the central barrier, as shown, for example, in Figs. 7 and 9. Previously, aspects of separatrix reconnection were studied by [6, 10, 5, 8, 9]. In the first subsection we apply to the standard nontwist map a known method [6] for obtaining reconnection criteria of period-one and period-two orbits. In the second subsection, a new general criterion for computing the reconnection thresholds of higher order ($n > 2$) periodic orbits is presented and applied.

3.1 Period-one and period-two separatrix reconnection

Figure 5 displays the standard nontwist map for three different sets of (a, b) values. The change in topology observed is due to the separatrix reconnection of period-one resonances that are located in the vicinity of the central region. To derive the reconnection threshold, observe that the first order resonances nearest to the central barrier can be described by the Hamiltonian

$$H(x, y) = -ay + \frac{a}{3}y^3 + \frac{b}{2\pi}\cos 2\pi x \ . \tag{23}$$

The period-one orbits are located at $(x, y) = (0, \pm 1)$ and $(1/2, \pm 1)$, and reconnection takes place when the hyperbolic orbit emerging from $(-1/2, -1)$ joins the hyperbolic point at $(0, 1)$.

In order for this to happen the value of the Hamiltonian must be the same at both points, i.e. $H(-1/2,-1) = H(0,1)$. This condition gives the reconnection threshold: $b = 4\pi a/3$. Due to the scaling of the x variable used here, this threshold has an extra factor of 2π as compared to the result reported in [5], and is equivalent to that reported previously in [6] for the logistic twist map. When $b < 4\pi a/3$ the map should exhibit an heteroclinic type topology, whereas for parameter values satisfying $b > 4\pi a/3$ the map should possesses an homoclinic type topology. We have numerically tested the reconnection threshold: for small values of a and b the reconnection process is clearly observed (cf. Fig. 5). For large parameter values, the map exhibits widespread stochasticity and the concept of reconnection has no visible meaning. For intermediate parameter values, the stochastic layer of the primary islands is visible and so it would be more appropriate to refer to this process as *stochastic layer reconnection.*

The reconnection scenario for even n is different from that for odd n. As shown in Figs. 6 and 7, reconnection occurs when two hyperbolic points collide on a symmetry line. Now we consider the special case of $n = 2$, for which an analytic threshold can be derived. The periodic-two orbits on s_1 are located at $(0, \pm\sqrt{1 - 1/(2a)})$. Note that the location of these orbits is independent of the value of b, a degenerate situation that only occurs for $n \leq 2$. To find the periodic orbits on s_3, consider a point (x_1, y_1) initially on s_3; i.e., $x_1 = a(1 - y_1^2)/2$. According to the involution formalism, this point will be a period-two orbit if $(x_2, y_2) \in s_4$; i.e., if $x_2 = a(1 - y_2^2)/2 + 1/2$, where $x_2 = x_1 + a(1 - y_2^2)$ and $y_2 = y_1 - b\sin(2\pi x_1)$. In general, there will be two solutions of these equations, $(x_1^{\pm}, y_1^{\pm})$, corresponding to the up and down periodic orbits on s_3. Since these orbits are hyperbolic, reconnection occurs when they collide; that is, when there is only one such solution (x_1, y_1) to the previous equations. It easy to check that for $b = 2\sqrt{1 - 1/2a}$ only one solution exists, $(x_1, y_1) = (1/4, b/2)$, and therefore this is the reconnection threshold. This reconnection threshold, which is equivalent to the one obtained in [6] for the logistic twist map, agrees quite well with the numerical results,

especially when there is not a lot of chaos and the separatrices are well defined (cf. Fig. 6).

3.2 Higher order separatrix reconnection

Consider now separatrix reconnection of higher ($n > 2$) periodic orbits. For even n the computation of the reconnection threshold can be done using the same idea as that used for period-two orbits: one just has to find the (a, b) values for which the hyperbolic orbits on the appropriate symmetry line collide. For example, for $a = 0.2625$ the collision of the $1/4$ hyperbolic orbits on s_1 occurs at $b = 0.4364$. These threshold values agree very well with the numerical results of Fig. 7, where the complete evolution of the $1/4$ periodic orbits is shown.

The computation of the threshold in the general case of odd n is more difficult; in what follows, we propose an approximate criterion. Consider periodic orbits with rotation number m/n with n odd. In this case, on each symmetry line, there is one elliptic orbit and one hyperbolic orbit. Without loss of generality, assume that the down periodic orbit on s_1 is the hyperbolic orbit (cf. Fig. 9), and let $\mathbf{x}_1 = (x_1, y_1)$ be its coordinates. Let $\mathbf{x}_2 = (x_2, y_2)$ denote the coordinates of the m/n up hyperbolic periodic orbit closest to s_1. The magnitude of the slope of the line joining $\mathbf{x}_1$ and $\mathbf{x}_2$ is $\mu(a, b) = |(y_2 - y_1)/(x_2 - x_1)|$. Let L be the matrix representing the linearization of the map at $\mathbf{x}_1$ and let $\mathbf{v} := (v_1, v_2)$ be the unstable eigenvector; i.e., $L\mathbf{v} = \lambda\mathbf{v}$ with $\lambda > 1$. Then, the magnitude of the slope of the unstable manifold at $\mathbf{x}_1$ is $\nu(a, b) = |v_2/v_1|$. According to the criterion proposed, the reconnection threshold is given by the set of (a, b) values for which the slope of the unstable manifold of the down hyperbolic point matches the slope of the line joining the up and the down hyperbolic points; that is, when $\mu(a, b) = \nu(a, b)$.

As an example consider the case when $m/n = 3/5$. In Fig. 8 we have plotted the magnitude of the slope of the line joining the two hyperbolic points, μ, and the magnitude of the slope of the unstable manifold, ν, as functions of a for fixed $b = 0.4215$. For $a < 0.6183$

$(a > 0.6183)$, $\nu < \mu$ $(\nu > \mu)$, and the topology is homoclinic (heteroclinic). The predicted reconnection threshold is $(a, b) = (0.6184, 0.4215)$, which agrees well with the numerically determined threshold $(a, b) = (0.6180, 0.4215)$, as shown in Fig. 9 (b). Typically, area preserving maps exhibit a self-similar hierarchy of ever higher order resonances. In the nontwist map this hierarchy includes successive changes in the topology, as seen for example in Fig. 10. The systematic study of this hierarchy of topology changes is a fascinating open problem, one that we plan to address in a future publication.

4 Transition to Chaos

Now we consider the destruction of the shearless KAM curve, i.e. the transition to chaos in the standard nontwist map. We restrict to the case in which the rotation number of this curve equals the inverse golden mean $1/\gamma = (\sqrt{5} - 1)/2$. In the first subsection the approximation by periodic orbits for the standard nontwist map is discussed and the shearless KAM curve defined. In the second subsection, the parameter values for the destruction of the shearless curve are computed using the residue criterion.

4.1 Approximation by periodic orbits—the shearless curve

The approximation of a KAM curve by periodic orbits requires finding a sequence of periodic orbits with corresponding rotation numbers $\{m_i/n_i\}$ that limit to the (irrational) rotation number, ω, of the curve that is to be approximated: $\omega = \lim_{i\to\infty} m_i/n_i$. In the limit, the periodic orbits approximate the KAM curve in the phase space as the sequence of rational numbers $\{m_i/n_i\}$ approach the irrational number ω [11].

In the standard nontwist map, the approximation by periodic orbits presents some difficulties since, contrary to what happens in twist maps, not all of the desired periodic orbits exist. To illustrate this, consider the approximation of the $1/\gamma$ KAM curve in the special case when $(a, b) = (1/\gamma, 0)$. In this case the standard nontwist map is integrable and the

$1/\gamma$ KAM curve is the shearless curve. In general, the best approximation by rationals of an irrational number ω is given by the convergents obtained from successive truncations of the continued fraction representation of ω [35]. In the case when $\omega = 1/\gamma$ the convergents are given by the sequence of Fibonacci ratios $\{F_{i-1}/F_i\}$, where F_i is the i-th Fibonacci number with $F_0 = F_1 = 1$ and $F_i = F_{i-1} + F_{i-2}$. Accordingly, to approximate the $1/\gamma$ KAM curve we need, in principle, to find periodic orbits with rotation numbers $\{m_i/n_i\} = \{F_{i-1}/F_i\}$. However, in the standard nontwist map, for $(a, b) = (1/\gamma, 0)$, only periodic orbits with $m/n < 1/\gamma$ exist and therefore in the approximation we have available only half of the Fibonacci sequence $\{m_i/n_i\} = \{F_{2i-1}/F_{2i}\}$. This is because, for any i, $F_{2i}/F_{2i+1} > 1/\gamma$ and $F_{2i-1}/F_{2i} < 1/\gamma$. For arbitrary values of (a, b) it is not trivial to decide which of the elements of the Fibonacci sequence correspond to periodic orbits that exist. However, if the (a, b) values are on appropriate bifurcation curves the problem becomes considerable simpler: if (a, b) is on the F_{2N}/F_{2N+1}-bifurcation curve, then all the periodic orbits with rotation numbers corresponding to the half-Fibonacci sequence $\{F_{2i-1}/F_{2i}\}$ for $i = 1, 2, \ldots, N$ exist, as well as all the periodic orbits with rotation numbers belonging to the full-Fibonacci sequence $\{F_k/F_{k+1}\}$ for $k = 2N + 1, 2N + 2, \ldots$.

An important thing to realize is that for (a, b) values on the F_{2N}/F_{2N+1}-bifurcation curve there are *two* $1/\gamma$ KAM curves. This is clearly seen in the limit $b = 0$ for which there is one $1/\gamma$ curve going through $(0, -\sqrt{1 - 1/(a\gamma)})$, the down curve, and another going through $(0, \sqrt{1 - 1/(a\gamma)})$, the up curve. The up and down KAM curves are approximated by the up and down periodic orbits, respectively. For (a, b) values on the F_{2N}/F_{2N+1}-bifurcation curve (cf. Fig 4), the up and down KAM curves (when they have not been destroyed) are separated by a finite distance proportional to $|F_{2N}/F_{2N+1} - 1/\gamma|$. Accordingly, as N increases, the distance between the up and down $1/\gamma$ KAM curves approaches zero and in the limit $N \to \infty$ both curves merge and become the $1/\gamma$ shearless curve. In this limit the F_{2N}/F_{2N+1}-bifurcation curves converge to the $1/\gamma$-bifurcation curve $b = \Phi_{1/\gamma}(a)$; that

is, $\Phi_{1/\gamma}(a) := \lim_{i\to\infty} \Phi_{F_i/F_{i+1}}(a)$ (cf. Fig. 4). By construction, for (a,b) values on $\Phi_{1/\gamma}$ the rotation number of the shearless curve equals $1/\gamma$.

To define the shearless curve, consider (a,b) values on the $\Phi_{1/\gamma}$ bifurcation curve and let y_i^u and y_i^d be the y-coordinates of the up and down periodic orbits, respectively, on the s_1 symmetry line, with rotation number F_{2i-1}/F_{2i}. Then, the $1/\gamma$ shearless curve is defined as the orbit with the initial condition $(0, y_{sh})$, where $y_{sh} := \lim_{i\to\infty} y_i^u = \lim_{i\to\infty} y_i^d$. That is, for $(a,b) \in \Phi_{1/\gamma}$, the $1/\gamma$ shearless curve is bracketed by the F_{2i-1}/F_{2i} up and the F_{2i-1}/F_{2i} down orbits (cf. Fig. 11).

4.2 Destruction of the shearless curve

The objective of this section is to use the residue criterion to find the critical parameter values, (a_c, b_c), for the destruction of the $1/\gamma$ shearless curve. In order for this to be a well-posed problem the $1/\gamma$ shearless curve must be defined for all the (a,b) values considered. Accordingly, in the search for the critical point (a_c, b_c), we are constrained to the one dimensional set $(a,b) = (a, \Phi_{1/\gamma}(a))$ defined by the $1/\gamma$-bifurcation curve.

The *residue criterion* [11] establishes a correspondence between the existence of a KAM curve and the stability of the periodic orbits that approximate it. Let $\{P_i\}$ be a sequence of periodic orbits, with corresponding residues $\{R_i\}$, approximating a KAM curve. Then, according to the residue criterion, if $\lim_{i\to\infty} R_i = 0$ then the KAM curve exists. On the other hand, if $\lim_{i\to\infty} R_i = \infty$, then the KAM curve does not exist. The residue criterion has been used successfully in many cases to predict, to remarkable precision, the threshold for the destruction of KAM curves. Recently, several theorems have been proved [36] that lend mathematical support to the criterion. The boundary in parameter space between the $R_i \to 0$ and the $R_i \to \infty$ regimes corresponds to the *critical state* in which the KAM curve is at the threshold of destruction. In this critical state the residue convergence exhibits nontrivial behavior. In the simplest cases (e.g. the standard map on the dominant symmetry line

[11]) $\lim_{i\to\infty} R_i = R^*$, where $R^* \neq 0, \infty$. However, more complicated residue convergence patterns are possible, in particular it is possible that, at criticality, the residues converge to a cycle $\{R_1^*, R_2^*, \ldots, R_n^*\}$. The residue convergence pattern is important because it is universal within families of maps. For example, there is a very large class of one-parameter area preserving twist maps that exhibit the *same* residue convergence pattern as that of the standard map, namely $\lim_{i\to\infty} R_i = 0.25$ (on the dominant symmetry line).

Relatively recently, nonstandard residue convergence patterns have been observed in standard-like maps with *two* harmonics (e.g. $x_{n+1} = x_n + y_{n+1}$, $y_{n+1} = y_n - c_1 \sin(2p\pi)x_n - c_2 \sin(2q\pi)x_n$ with p, q integers) [37, 38, 39, 40] and in piecewise-linear maps [41, 42]. The convergence pattern of the residues allows the classification of the fundamentally different ways in which a KAM curve can be destroyed. Our numerical results (which will be discussed in detail below) indicate that, at the threshold for destruction of the $1/\gamma$ shearless curve, the residues in the standard nontwist map exhibit a *period-six cycle* convergence pattern. This convergence pattern is different from that found in twist maps and it indicates that the transition to chaos in nontwist maps is fundamentally different from the transition to chaos in twist maps.

In order to systematically study the destruction of invariant curves in the standard nontwist map it is useful to know the *rules* governing the stability of periodic orbits on the different symmetry lines. To get these rules, note that from the map symmetry of Eq. (9),

$$\begin{aligned} R_{u_1} = R_{d_2}\,, \quad R_{d_1} = R_{u_2} \\ R_{u_3} = R_{d_4}\,, \quad R_{d_3} = R_{u_4}\,, \end{aligned} \tag{24}$$

where R_{u_i} (R_{d_i}) denotes the residue of the up (down) periodic orbit on s_i. On the other hand, the routing pattern of Eq. (21) implies,

$m/n =$ odd/even:

$$R_{u_1} = R_{u_2}\,, \quad R_{d_1} = R_{d_2}$$

$$R_{u_3} = R_{u_4}\,, \quad R_{d_3} = R_{d_4}$$

$m/n =$ odd/odd:

$$R_{u_1} = R_{u_4}\,, \quad R_{d_1} = R_{d_4}$$

$$R_{u_2} = R_{u_3}\,, \quad R_{d_2} = R_{d_3}$$

$m/n =$ even/odd:

$$R_{u_1} = R_{u_3}\,, \quad R_{d_1} = R_{d_3}$$

$$R_{u_2} = R_{u_4}\,, \quad R_{d_2} = R_{d_4}$$

From these relations it is straightforward to get the stability rules summarized in Table 1. There are three cases: $m/n =$ *odd/even*, *odd/odd* and *even/odd*. Note that for each m/n, there are only two independent residues, denoted by R_1 and R_2, that determine the stability properties of the up and down orbits on the four symmetry lines. This is an important result that will be used when studying residue convergence at the transition to chaos. Consistent with the numerical results of Fig. 3, periodic orbits on the same symmetry line with even n have the same stability properties. The table does not give information about the sign of the residues; however, numerical results indicate that close to the bifurcation point the residues of the up and down m/n periodic orbits with n odd satisfy $R_1 R_2 < 0$ and, for the particular case where m/n is of the form odd/odd, $R_1 = -R_2$.

Table 2 shows the residue convergence pattern at criticality in the standard nontwist map. Depending on the symmetry line under consideration, the convergence is either to the six-cycle $SC^+ := \{H_1, H_2, H_3,\ H_4, H_5, H_6\}$, or to the six-cycle $SC^- := \{G_1, G_2, G_3,\ G_4, G_5, G_6\}$, where H_i and G_i are real numbers which will be computed below. The first two columns of Table 2 list the rotation number label $[i] := F_i/F_{i+1}$ of the periodic orbits under consideration. The rest of the columns contain the values of the residues on the various symmetry lines, where, as before, R_{ui} (R_{di}) denotes the residue of the up (down) periodic orbit on the symmetry line s_i. From the Table 2 it follows that the residues of the up periodic orbits on s_1 and s_4 and the residues of the down periodic orbits on s_2 and s_3 converge to SC^-. On the other hand, the residues of the down periodic orbits on s_1 and s_4 and the

residues of the up periodic orbits on s_2 and s_3 converge to SC^+. The two six-cycles are not independent. Using the stability rules, of Table 1, it follows that $G_1 = H_1$, $G_4 = H_4$, $G_3 = H_6$, and $G_6 = H_3$. Also, in each cycle, the second and fifth elements are the same: $G_2 = G_5$ and $H_2 = H_5$. Finally, there is numerical evidence that $G_2 = -H_2$; therefore, the only independent residues are H_1, H_2, H_3, H_4, and H_6.

Finding the numerical values of the elements of the six cycles is difficult because only half of the Fibonacci sequence is available and because the cycle of residues has period six. For example, to complete the six-cycle twice it is necessary to find periodic orbits up to $m/n = 46368/75025$, and this give us only two residues to compare for each H_i. To complete the cycle three times it is required to find periodic orbits with rotation numbers m/n up to $14,930,352/25,152,817$ which is basically an impossible task due to computational limitations. However, a closer look at the residue convergence pattern of Table 2 shows that with periodic orbits up to $m/n = 46368/75025$, there are four residues to compare for each H_i. The key is to realize that the convergence to the six-cycle along different symmetry lines has a "phase shift" of three. As an example, consider convergence to H_1. From Table 2 it is clear that, at the critical value, the residues of the $1/2$ and $377/610$ down periodic orbits on s_1 must be the same and equal to H_1. The important thing to realize is that the residues of the $21/34$ and $6765/10946$ up periodic orbits on s_3 must also be equal to H_1 and, therefore, we have four residues to compare to get the convergence to H_1. Similar ideas can be used for the computation of H_2, H_3, H_4, and H_6.

The precise determination of the critical parameter values (a_c, b_c) is a delicate calculation because two problems must be solved at once: the construction of the $1/\gamma$-bifurcation curve and the determination of the values of (a, b) on this curve for which the residues show convergence to the six-cycle. The $1/\gamma$-bifurcation curve can be computed using the fact that, as a consequence of the period-six cycle of the residues, the bifurcation curves, for

(a, b) values near criticality, satisfy the following *scaling relation*:

$$\Phi(a)_{[n]} = \Phi(a)_{1/\gamma} + B(n)\lambda^{-n}\,, \tag{25}$$

where $\Phi(a)_{[n]}$ denotes the $[n] := F_n/F_{n+1}$–bifurcation curve, λ is a constant and $B(n)$ is a *period-twelve* function, i.e. $B(n+12) = B(n)$. Evidence of this scaling relation is presented in Table 3, where the values of $B(n)$ are shown. Note that, the scaling function has period-twelve, whereas the residues have period-six. This is because the approximation of the $1/\gamma$-bifurcation curve employs the full Fibonacci sequence, whereas the approximation of the $1/\gamma$ shearless KAM curve employs only the half Fibonacci sequence, i.e. period-six in the half Fibonacci sequence corresponds to period-twelve in the full Fibonacci sequence.

From the scaling relation of Eq. 25 it follows that

$$\Phi_{1/\gamma}(a) = \lim_{n\to\infty} \frac{\Phi_{[n+1]}\Phi_{[n+12]} - \Phi_{[n]}\Phi_{[n+13]}}{\left(\Phi_{[n+1]} - \Phi_{[n]}\right) - \left(\Phi_{[n+13]} - \Phi_{[n+12]}\right)}\,. \tag{26}$$

We have numerically computed bifurcation curves $\Phi_{[N]}$ up to $[N] = [24] = 75,025/121,393$ (note that $|75,025/121,393 - 1/\gamma| \approx 10^{-11}$). With these numerical values, $\Phi_{1/\gamma}$ was approximated using Eq. 26: $\Phi_{1/\gamma} \approx (\Phi_{[12]}\Phi_{[23]} - \Phi_{[11]}\Phi_{[24]})/((\Phi_{[12]} - \Phi_{[11]}) - (\Phi_{[24]} - \Phi_{[23]}))$; all the values of $\Phi_{1/\gamma}$ reported in this paper were computed using this expression. Table 4 summarizes the numerical results for the determination of the critical parameter values (a_c, b_c) and the values of the six-cycle. The table has five rows, one for each independent element of the six-cycle: H_1, $H_2 = H_5$, H_3, H_4, and H_6. The first column gives the element of the six-cycle, the second column gives the rotation number $[i] = F_{2i-1}/F_{2i}$, and the third column gives the residue under consideration. The last three columns indicate the numerical values of the residues for $(a^-, b^-) = (0.686048, 0.742489259544)$, $(a_c, b_c) = (0.686049, 0.742493131039)$, and $(a^+, b^+) = (0.686050, 0.742497002412)$, respectively. All these (a, b) values are on the $1/\gamma$-bifurcation curve. The numerical results of the table are plotted in Fig. 12. For $(a, b) = (a^+, b^+)$, the residues of higher convergents increase in magnitude and, therefore,

this value is above criticality. On the other hand, (a^-, b^-) is below the critical value because the successive values of the residues are successively smaller. The results indicate that the intermediate case

$$(a_c, b_c) = (0.686049000000,\ 0.742493131039) \tag{27}$$

is the critical value for destruction of the $1/\gamma$ shearless curve and, therefore, convergence to the six-cycle. From the numerical results of Table 4 we get the following values for the elements of the six cycle:

$$H_1 = 2.325 \pm 0.002 \qquad H_2 = 2.575 \pm 0.020 \tag{28}$$

$$H_3 = -0.599 \pm 0.010 \qquad H_4 = -1.283 \pm 0.001 \tag{29}$$

$$H_5 = 2.575 \pm 0.020 \qquad H_6 = 1.548 \pm 0.037\,. \tag{30}$$

In Fig. 13 we have plotted the standard nontwist map at the critical value (a_c, b_c) for the destruction of the $1/\gamma$ shearless curve and convergence to the six-cycle. Observe the high degree of stochasticity in the map; all elliptic orbits seem to have disappeared leaving a "stochastic sea" with a well-defined "shore" given by the shearless $1/\gamma$ orbit. In the figure, several initial conditions below the shearless curve wander stochastically in the bottom part of the phase space but do not cross the shearless orbit. To display the metamorphosis of the $1/\gamma$ shearless curve as the (a, b) values are increased, this curve is plotted in Fig. 14 for (a, b) values below criticality, at criticality, and above criticality. To show evidence of the destruction of the shearless curve, Fig. 14(c) also shows the up and down periodic orbits with $m/n = 987/1597$. The fact that the chaotic orbit shown in the picture crosses these periodic orbits indicates the destruction of the shearless curve.

To analyse the structure of the $1/\gamma$ shearless orbit at criticality, this orbit is plotted in Figs. 15(a)–(b) using *symmetry line coordinates* centered at the point where the shearless orbit intersects s_3: $\widetilde{x} = x - a(1 - y^2)/2$, $\widetilde{y} = y - y_s$, where $y_s = 0.222521$. Figure 15(a)

displays the shearless orbit in the right-upper quadrant of phase space, and Fig. 15(b) is a magnification of Fig. 15(a) by a factor of 323.5 in the x-direction and a factor of 471.7 in the y-direction. This magnification is quite big; the area of the phase space region depicted in Fig. 15(a) is about 150,000 time larger than the area of the phase space region shown in Fig. 15(b). It was shown in [12, 13] that in the standard map, critical invariant curves exhibit self-similar structure. The remarkable similarity of Figs. 15(a) and 15(b) indicates that, in the nontwist map, the $1/\gamma$ shearless curve has a self-similar structure. Note that the scaling factors of the critical $1/\gamma$ shearless curve are different from the scaling factors of the $1/\gamma$ KAM curve in twist maps. In the forthcoming publication [14] we analyze the critical behavior of the shearless curve using the renormalization group formalism.

5 Conclusions

In this paper we have presented a study of periodic orbits and the transition to chaos in area preserving nontwist maps, maps that violate the twist condition of Eq. (3). Many mathematical results regarding KAM curves in nontwist maps remain to be established. Due to the violation of the twist condition, important theorems such as the KAM theorem [4], cannot be applied to this problem. One of the main contributions of this paper is a detailed numerical study of the destruction of the so-called shearless curve, the KAM curve located where the twist condition fails. The understanding of when and how a KAM curves breaks has important physical implications because, in two-dimensions KAM curves are transport barriers; their breakup heralds the lack of confinement in the system. In particular, the study of the shearless curve in nontwist maps sheds light on the transport and mixing properties of plasma and fluid systems.

The study presented here has been based on the standard nontwist map, which is a simple prototype nontwist map. The study of the transition to chaos relied upon the use of periodic orbits to determine the existence of KAM curves. For this reason a discussion

of periodic orbits in the standard nontwist map was presented, prior to the study of the transition to chaos. Contrary to what typically happens in twist maps, periodic orbits in the nontwist map (when they exist) come in pairs; that is, there are two periodic orbits with the same rotation number on each symmetry line. As the map parameters change, the two periodic orbits on the same symmetry line can approach each other and can eventually collide. The periodic orbit collision phenomenology was described in detailed. Periodic orbit collisions lead, eventually, to periodic orbit annihilation, which is problematic when one is using periodic orbits to approximate KAM curves. The main difficulty being that, in general, it is not known a priori which periodic orbits exists and which have been destroyed. To handle this problem the concept of bifurcation curves in (a, b) space was introduced. The main virtue of these bifurcation curves is that for (a, b) values below the r/s-bifurcation curve, periodic orbits with $m/n < r/s$ exist.

Another important bifurcation discussed in this paper is separatrix reconnection, which is a global bifurcation that changes the phase space topology in the vicinity of the shearless curve. Following a discussion of period-one and period-two reconnection, we presented a general approximate criterion for predicting the threshold for higher order separatrix reconnection. The precise role of separatrix reconnection in the destruction of the shearless curve remains to be elucidated. In going from the heteroclinic-type topology (cf. Fig. 9(a)) to the homoclinic-type topology (cf. Fig. 9(c)) the shearless curve seems to break and reconnect. The relationship between these topology changes of the shearless curves and the destabilization of nearby periodic orbits remains to be clarified.

Following the discussion of periodic orbits, the problem of the transition to chaos due to the destruction of the shearless curve, was addressed in Sec. 4. In the integrable limit of the standard nontwist map ($b = 0$), the shearless curve is the line $y = 0$, along which the twist condition is violated. In the nonintegrable case ($b \neq 0$), the shearless curve was defined using approximation by periodic orbits. Intuitively, the shearless orbit is the orbit located in the

region were the twist condition is locally violated. The threshold for the destruction of the shearless KAM curve with rotation number equal to the inverse golden mean was determined using the residue criterion. After studying the stability rules of the periodic orbits, it was shown that, contrary to what happens in twist maps, at the threshold of destruction, the residue of the periodic orbits approximating the $1/\gamma$ shearless curve converge to a period-six cycle. Using the scaling properties of the bifurcation curves near the critical point, the $1/\gamma$ bifurcation curve was constructed and the critical parameter values determined as well as the numerical values of the elements of the six-cycle. It was shown that at the critical point, the $1/\gamma$ shearless curve exhibits self-similar structure which is different for that of twist maps. In the future paper [14] this will be reinterpreted as a period-twelve fixed point of the renormalization operator with two unstable eigenvalues.

Acknowledgment

This work was funded by the US Dept. of Energy under No. DE-FG05-80ET-53088. One of us (DdCN) acknowledges support by the Universidad Nacional Autonoma de México and thanks R. de la Llave for helpful conversations.

References

[1] J. Moser, *Stable and Random Motion in Dynamical Systems* (Princeton University Press, Princeton New Jersey, 1973).

[2] R.S. MacKay and J.D. Meiss (eds.), *Hamiltonian Dynamical Systems: a reprint selection* (Adam-Hilger, London, 1987).

[3] J.D. Meiss, Rev. Mod. Phys. 64 (1992) 795.

[4] J. Moser, Nach. Akad. Weiss. Gottingen, Math. Phys. K1 IIa (1962) 1.

[5] D. del-Castillo-Negrete and P.J. Morrison, Phys. Fluids A 5 (1993) 948.

[6] J.E. Howard and S.M. Hohs, Phys. Rev. A 29 (1984) 418.

[7] J.B. Weiss, Phys. Fluids A 3 (1991) 1379.

[8] D. del-Castillo-Negrete, Dynamics and Transport in Rotating Fluids and Transition to Chaos in Area Preserving Nontwist maps, Ph.D thesis, The University of Texas, Austin, October, 1994.

[9] J.E. Howard and J. Humpherys, Physica D 80 (1995) 256.

[10] J.P. Van der Weele and T.P. Valkering, Physica A 169 (1990) 42.

[11] J.M. Greene, J. Math. Phys. 20 (1979) 1183.

[12] L.P. Kadanoff, Phys. Rev. Letter 47 (1981) 1641.

[13] S.J. Shenker and L.P. Kadanoff, J. Stat. Phys. 27 (1982) 631.

[14] D. del-Castillo-Negrete, J. Greene, and P.J. Morrison, Area Preserving Nontwist Maps: Renormalization Approach to the Transition to Chaos, to be submmited to Physica D.

[15] R.S. MacKay, Renormalization in Area Preserving Maps, Thesis, Princeton 1982 (Univ. Microfilms Int., Ann Arbor MI).

[16] R.S. MacKay, Physica D 7, (1983) 283.

[17] J.M. Greene, The Status of KAM Theory from a Physicist's Point of View. General Atomics Project 4927, January 1990.

[18] J.M. Ottino, *The Kinematics of Mixing: Stretching, Chaos, and Transport* (Cambridge Texts in Aplied Mathematics, Cambridge UniversityPress, 1989).

[19] D. del-Castillo-Negrete and P.J. Morrison, Bull. Am. Phys. Soc. 37 (1992) 1543.

[20] D. del-Castillo-Negrete and P.J. Morrison, Hamiltonian Chaos and Transport in Quasi-geostrophic Flows, in *Chaotic Dyanamics and Transport in Fluids and Plasmas*, ed. I. Prigogine, (American Institute of Physics, New York, 1993).

[21] R.P. Behringer, S.D. Meyers and H.L. Swinney, Phys. Fluids A 3 (1991) 1243.

[22] R.T. Pierrehumbert, Phys. Fluids A 3 (1991) 1250.

[23] R.D. Hazeltine and J.D. Meiss, *Plasma Confinement* (Lectures Notes in Physics Vol. 86, Addison-Wesley, 1992).

[24] T.H. Stix, Phys. Rev. Lett. 36 (1976) 10.

[25] M. Hugon, et al., Nuclear Fusion 32 (1992) 33.

[26] E.J. Doyle, et al., Physics of Fluids B 3 (1991) 2300.

[27] W. Horton, Phys. Reports 192 (1990) 1.

[28] W.T. Kyner Mem. of the Am. Math. Soc. 81, (1968) 1.

[29] G.M. Zaslavsky, R.Z. Sagdeev, D.A. Usikov and A.A. Chernikov, *Weak Chaos and Quasi-Regular Patterns* (Cambridge Nonlinear Science Series, Cambridge University Press, 1991)

[30] S.S. Abdullaev, CHAOS 4 (1994) 569.

[31] K.R. Symon and A.M. Sessler, in Proc. Int. Conf. on High-Energy Accelerators and Instrumentation (CERN, Geneva, 1956) p. 44; A. Gerasimov, F.M. Israilev, J.L. Tennyson and A.B. Temnykh, Springer Lecture Notes in Physics, vol. 247 (1986) 154.

[32] J.E. Howard, A.J. Lichtenberg, M.A. Lieberman and R.H. Cohen, Physica D 20 (1986) 259.

[33] R. de Vogelaere, *Contributions to the Theory of Nonlinear Oscillations*, edited by S. Lefschetz (Princeton U.P., Princeton, New Jersey, 1958), Vol. IV. p.53.

[34] G.D. Birkhoff, *Dynamical Systems* (AMS Colloq. Publ., vol. 9, revised 1966).

[35] I. Niven and H.S. Zuckerman, *An Introduction to the Theory of Numbers*, third edition (John Wiley & Sons, New York, 1972).

[36] C. Falcolini and R, de la Llave, J. Stat. Phys. 67 (1992) 609.

[37] J.M. Greene, H. Johannesson, B. Schaub and H. Suhl, Phys. Rev. A 36 (1987) 5858.

[38] J.A.Ketoja and R.S. MacKay, Physica D 35, (1989) 318.

[39] J.M. Greene, J. Mao, Nonlinearity 3 (1990) 69.

[40] J. Wilbrink, Nonlinearity 3 (1990) 567.

[41] J. Wilbrink, Physica D 26 (1987) 358.

[42] J. Wilbrink, Phys. Letters A 131 (1988) 251 .

FIGURE CAPTIONS

FIG. 1. Symmetry lines of the standard nontwist map, which are used to reduce the computation of periodic orbits to a *one-dimensional* root finding problem. Generically, for each m/n there are two periodic orbits, called the up and down orbits, on each symmetry line.

FIG. 2. Periodic orbit collision for $m/n = 3/5$ on the s_1 symmetry line. For $b < 0.44$ there are two periodic orbits; at the bifurcation value $b = 0.44$ they collide and for $b > 0.44$

the orbits no longer exist. The bifurcation value depends on a and m/n. The shape of the bifurcation curve shown here is typical of periodic orbit collisions.

FIG. 3. Residues of up and down periodic orbits on s_1 with $m/n = 3/5,\ 8/13$ and $21/34$ as functions of a for fixed $b = 0.7425$. At the bifurcation point the residues of the up and down periodic orbits are zero. Close to the bifurcation point periodic orbits with n odd (even) have different (the same) stability type. For m/n of the form *odd/even* the residues of the up and down periodic orbits are equal.

FIG. 4. The r/s-bifurcation curves, $b = \Phi_{r/s}(a)$, for $r/s = 2/3,\ 3/5,\ 5/8,\ 8/13$ and $21/34$. These curves are the locus of (a, b) points for which the r/s-periodic orbits collide. For (a, b) values below $b = \Phi_{r/s}(a)$, periodic orbits with $m/n < r/s$ are below the collision threshold, and therefore these orbits exist. The bifurcation curves shown in this figure converge to the $1/\gamma$ bifurcation curve which is the locus of (a, b) values for which the rotation number of the shearless curve is equal to $1/\gamma$.

FIG. 5. Separatrix reconnection of period-one resonances in the standard nontwist map. In case (a), $(a, b) = (0.080, 0.125)$ and the map displays the heteroclinic topology. The homoclinic topology is shown in case (c) for which (0.024,0.300). Case (b) displays the reconnection point, which in good accord with the reconnection threshold formula, $b = 4\pi a/3$, has $(a, b) = (0.048, 0.2000)$. This reconnection pattern is generic for m/n periodic orbits with n odd.

FIG. 6. Separatrix reconnection of period-two resonances in the standard nontwist map. In (a), $(a, b) = (0.51, 0.25)$ and the map displays the heteroclinic topology. The dipole topology is shown in (c), for which (0.51,0.31). Case (b) displays the reconnection point, which in good accord with the reconnection threshold formula, $b = 2\sqrt{1 - 1/(2a)}$, has $(a, b) = (0.51, 0.28)$. This reconnection pattern is generic for

m/n periodic orbits with n even.

FIG. 7. Separatrix reconnection and periodic orbit annihilation for $m/n = 1/4$. In case (a), $(a, b) = (0.2625, 0.4400)$ and the topology is heteroclinic. Hyperbolic orbit collision and separatrix reconnection are shown in case (b), for which $(a, b) = (0.2625, 0.4364)$. Case (c) displays the dipole formation at $(a, b) = (0.2625, 0.4500)$, after the hyperbolic collision. The annihilation of the $1/4$ periodic orbits is shown in case (d), for which $(a, b) = (0.2625, 0.4580)$. This is the typical pattern for m/n periodic orbits with n even.

FIG. 8. Comparison of unstable manifold slope and fixed point slope, for an $m/n = 3/5$ periodic orbit as function of a for fixed $b = 0.4215$. According to the criterion proposed, reconnection occurs when the two slopes match. Reconnection is predicted for $(a, b) = (0.6183, 0.4215)$, which is in good agreement with the threshold of Fig. 9.

FIG. 9. Separatrix reconnection and periodic orbit annihilation for $m/n = 3/5$. In case (a), $(a, b) = (0.6180, 0.4000)$ and heteroclinic topology is shown, while in (b), $(a, b) = (0.6180, 0.4215)$ and separatrix reconnection is shown. Case (c) displays the homoclinic topology with $(a, b) = (0.6180, 0.4300)$. The annihilation of the 3/5-periodic orbits due to periodic orbit collision is shown in case (d), for which $(a, b) = (0.6180, 0.4410)$. This is the typical pattern for m/n-periodic orbits with n odd. The reconnection values of case (b) agree well with the prediction of Fig. 8(b).

FIG. 10. The standard nontwist map at $(a, b) = (0.0716, 0.4500)$ illustrating the possibility of "nested topologies." On the first level, the period-one resonances display the homoclinic topology; at a higher level, resonances close enough to the shearless curve display the heteroclinic topology.

FIG. 11. Depiction of the periodic orbit approximation of the $1/\gamma$ shearless KAM curve. Shown are the first four elements of the half Fibonacci sequence. The up and down periodic orbits bracket the shearless curve.

FIG. 12. Residue convergence to the six-cycle $\{H_1, H_2, H_3, H_4, H_5, H_6\}$ for (a, b) values on the $1/\gamma$ bifurcation curve; above criticality (a^+, b^+) (circles), at criticality (a_c, b_c) [cf. (27)] (crosses), and below criticality (a^-, b^-) (squares). For the numerical values of H_i see Table 4.

FIG. 13. The standard nontwist map at the critical parameter values, $(a_c, b_c) = (0.686049000000, 0.74249313039)$, for destruction of the $1/\gamma$ shearless orbit.

FIG. 14. Shearless orbit (a) below criticality, (b) at criticality and (c) above criticality. The fact that, in case (c), the orbit shown crosses the up and down 987/1597 periodic orbits indicates that the shearless curve has been destroyed.

FIG. 15. Self-similar structure of the $1/\gamma$ shearless curves at criticality. In case (a) the shearless curve has been plotted in symmetry lines coordinates. Case (b) shows a magnification of (a) by a factor of 324 in the x-direction, and 472 in the y-direction.

TABLE CAPTIONS

TABLE 1. Stability rules for periodic orbits on the symmetry lines. There are three cases: $m/n = odd/even$, odd/odd and $even/odd$. In each case, only two residues, denoted here by R_1 and R_2, determine the residues of the up and down orbits on the four symmetry lines.

TABLE 2. Period-six convergence pattern of residues of the standard nontwist map for (a, b) values on the $1/\gamma$ bifurcation curve near criticality. The first two columns denote

the periodic orbit under consideration, where $[i] := F_i/F_{i+1}$. The residues of the up and down periodic orbits on the various symmetry lines converge to the six-cycles $\{H_1, H_2, \ldots H_6\}$ and $\{G_1, G_2, \ldots G_6\}$. These two six-cycles are not independent.

TABLE 3. Period-twelve behavior of the scaling function $B(n)$ of Eq. (25).

TABLE 4. Convergence of the residues to the six-cycle for (a, b) values on the $1/\gamma$-bifurcation curve. Each row corresponds to each independent element of the six cycle $\{H_1, H_2, H_3, H_4, H_5, H_6\}$. The third column denotes the residue under consideration, e.g. R_{d_j} denotes the residue of the down periodic orbit on the s_j symmetry line. The last three columns give the values of the residues below criticality, at criticality and above criticality respectively. These numerical results are plotted on Figure 12.

m/n = odd/even

	s_1	s_2	s_3	s_4
up orbit	R_1	R_1	R_2	R_2
down orbit	R_1	R_1	R_2	R_2

m/n = odd/odd

	s_1	s_2	s_3	s_4
up orbit	R_1	R_2	R_2	R_1
down orbit	R_2	R_1	R_1	R_2

m/n = even/odd

	s_1	s_2	s_3	s_4
up orbit	R_1	R_2	R_1	R_2
down orbit	R_2	R_1	R_2	R_1

TABLE 1

$[i]$	F_i/F_{i+1}	$R_{u1} = R_{d2}$	$R_{d1} = R_{u2}$	$R_{u3} = R_{d4}$	$R_{d3} = R_{4u}$
[1]	1/2	G_1	H_1	H_4	G_4
[3]	3/5	G_2	H_2	H_5	G_5
[5]	8/13	G_3	H_3	H_6	G_6
[7]	21/34	G_4	H_4	H_1	G_1
[9]	55/89	G_5	H_5	H_2	G_2
[11]	144/233	G_6	H_6	H_3	G_3
[13]	377/610	G_1	H_1	H_4	G_4
[15]	987/1597	G_2	H_2	H_5	G_5
[17]	2584/4181	G_3	H_3	H_6	G_6
[19]	6765/10946	G_4	H_4	H_1	G_1
[21]	17711/28657	G_5	H_5	H_2	G_2
[23]	46368/75025	G_6	H_6	H_3	G_3

TABLE 2

n	$B(n)$	n	$B(n)$
1	−0.917	13	−0.590
2	0.699	14	0.669
3	−0.542	15	−0.456
4	0.627	16	0.608
5	−0.508	17	−0.473
6	0.410	18	0.414
7	−0.596	19	−0.590
8	0.673	20	0.666
9	−0.856	21	−0.852
10	0.609	22	0.606
11	−0.474	23	−0.480

TABLE 3

			(a^-, b^-)	(a_c, b_c)	(a^+, b^+)
H_1	[1]	R_{d1}	2.778	2.778	2.778
	[7]	R_{u3}	2.397	2.398	2.398
	[13]	R_{d1}	2.317	2.328	2.338
	[19]	R_{u3}	2.169	2.323	2.488
H_2 H_5	[3]	R_{d1}	2.652	2.652	2.652
	[9]	R_{u3}	2.554	2.555	2.557
	[15]	R_{d1}	2.569	2.595	2.622
	[21]	R_{u3}	2.200	2.555	2.984
H_3	[5]	R_{d1}	−0.759	−0.759	−0.759
	[11]	R_{u3}	−0.593	−0.593	−0.594
	[17]	R_{d1}	−0.599	−0.609	−0.620
	[23]	R_{u3}	−0.442	−0.589	−0.786
H_4	[1]	R_{u3}	−1.633	−1.633	−1.633
	[7]	R_{d1}	−1.324	−1.325	−1.325
	[13]	R_{u3}	−1.279	−1.283	−1.288
	[19]	R_{d1}	−1.216	−1.282	−1.354
H_6	[5]	R_{u3}	1.706	1.706	1.707
	[11]	R_{d1}	1.570	1.574	1.577
	[17]	R_{u3}	1.536	1.585	1.637
	[23]	R_{d1}	0.937	1.510	2.517

TABLE 4

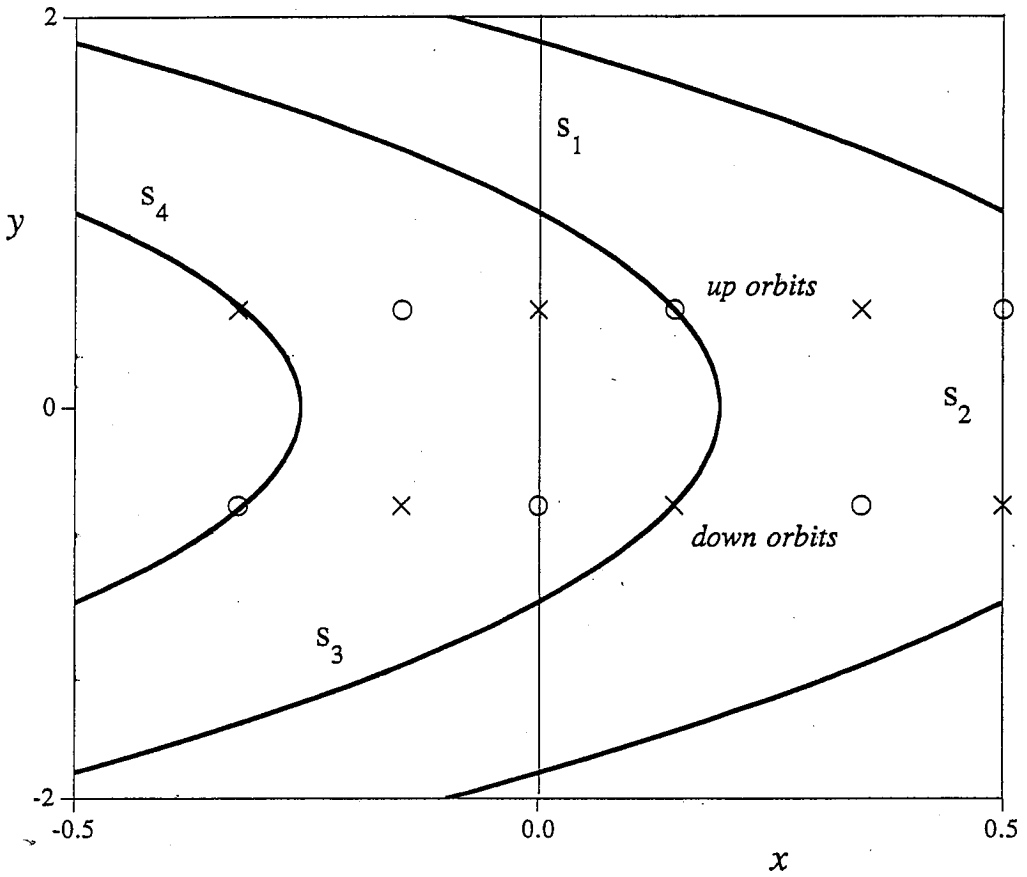

FIGURE 1

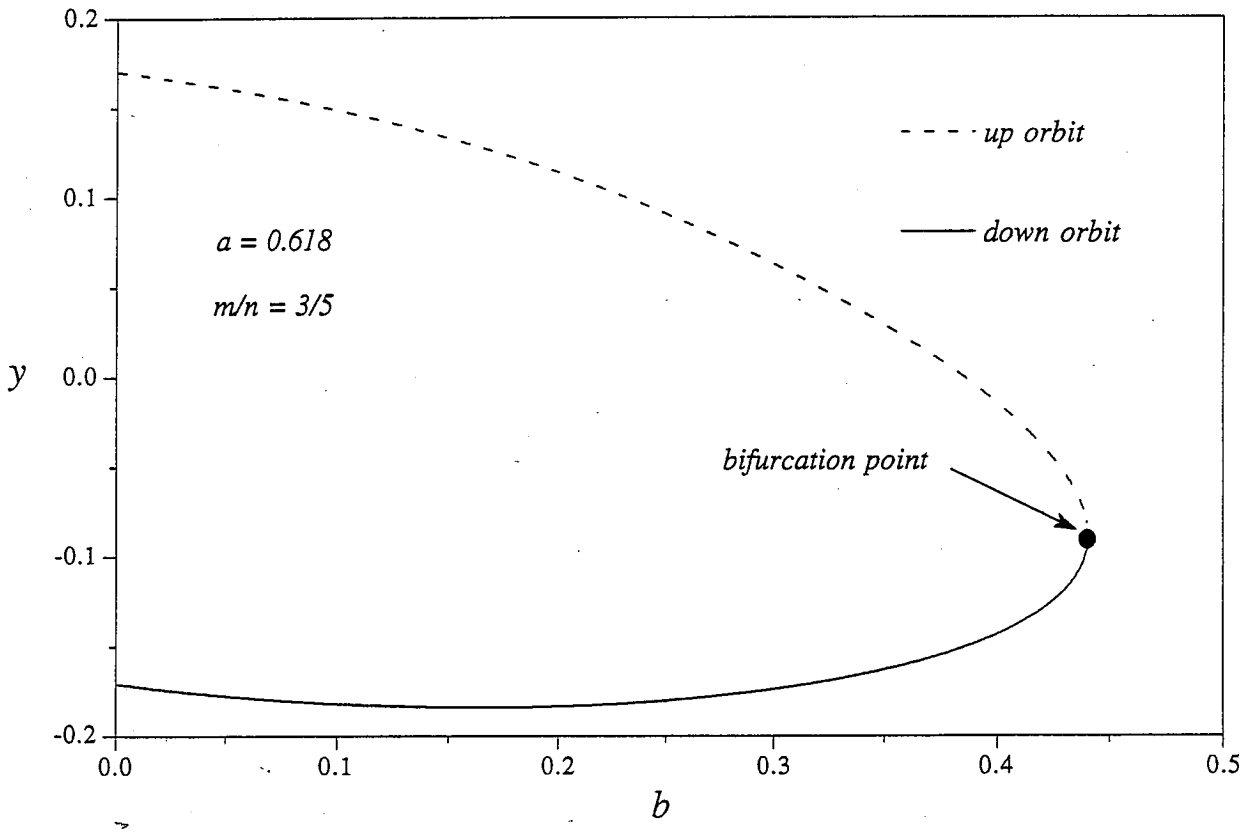
0.2
0.1
0.0
-0.1
-0.2
y
0.0
0.1
0.2
0.3
0.4
0.5
b
up orbit
down orbit
a = 0.618
m/n = 3/5
bifurcation point

FIGURE 2

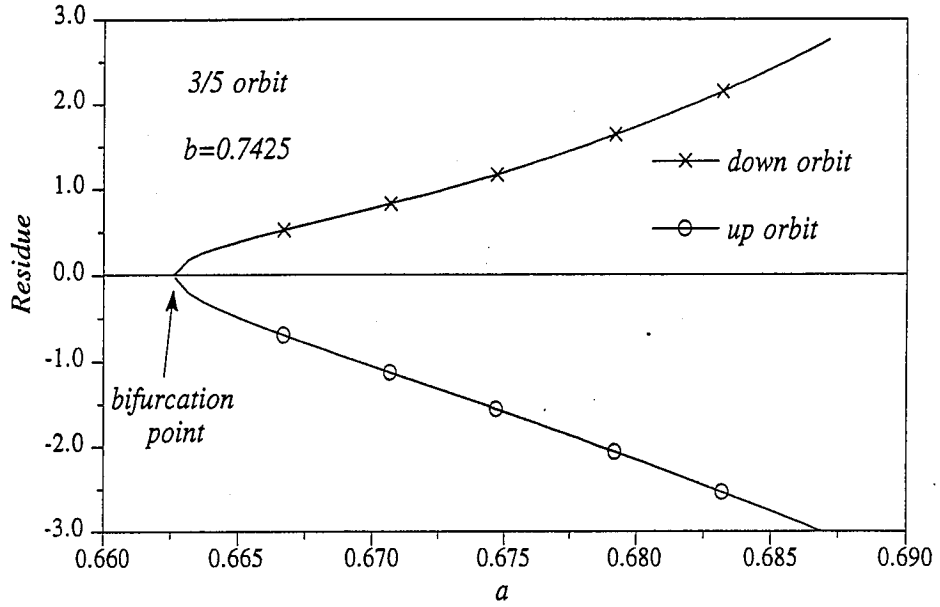
3/5 orbit
b=0.7425
down orbit
up orbit
bifurcation point
Residue
a
3.0
2.0
1.0
0.0
-1.0
-2.0
-3.0
0.660
0.665
0.670
0.675
0.680
0.685
0.690

(a)

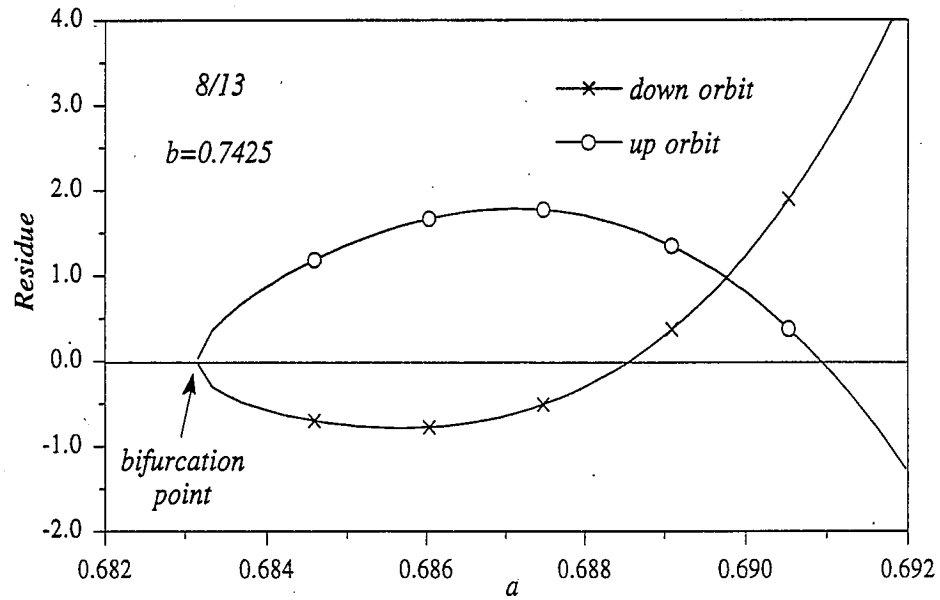
8/13
b=0.7425
down orbit
up orbit
bifurcation point
Residue
a
4.0
3.0
2.0
1.0
0.0
-1.0
-2.0
0.682
0.684
0.686
0.688
0.690
0.692

(b)

FIGURE 3

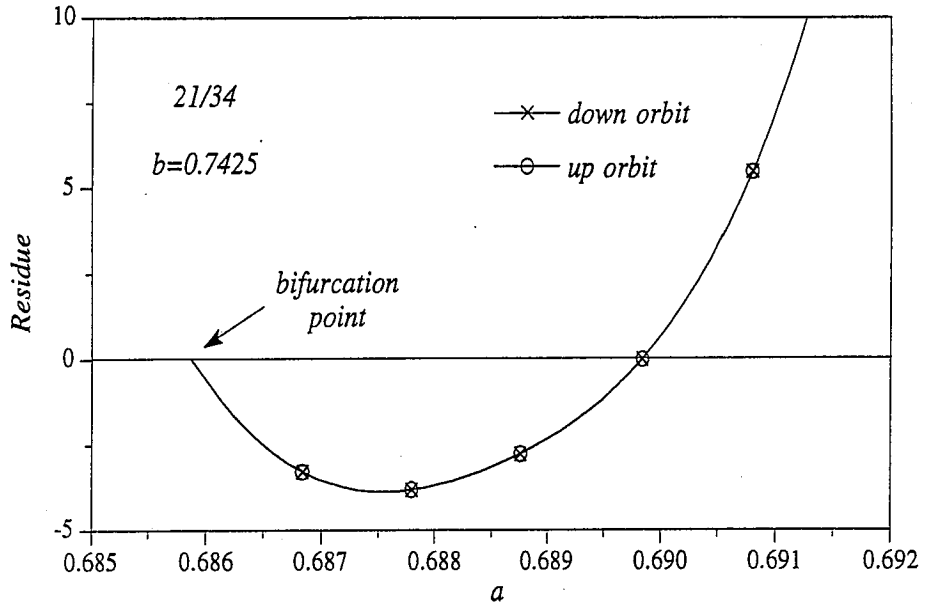
10
5
0
-5
Residue
21/34
b=0.7425
down orbit
up orbit
bifurcation
point
0.685
0.686
0.687
0.688
0.689
0.690
0.691
0.692
a

(c)

FIGURE 3

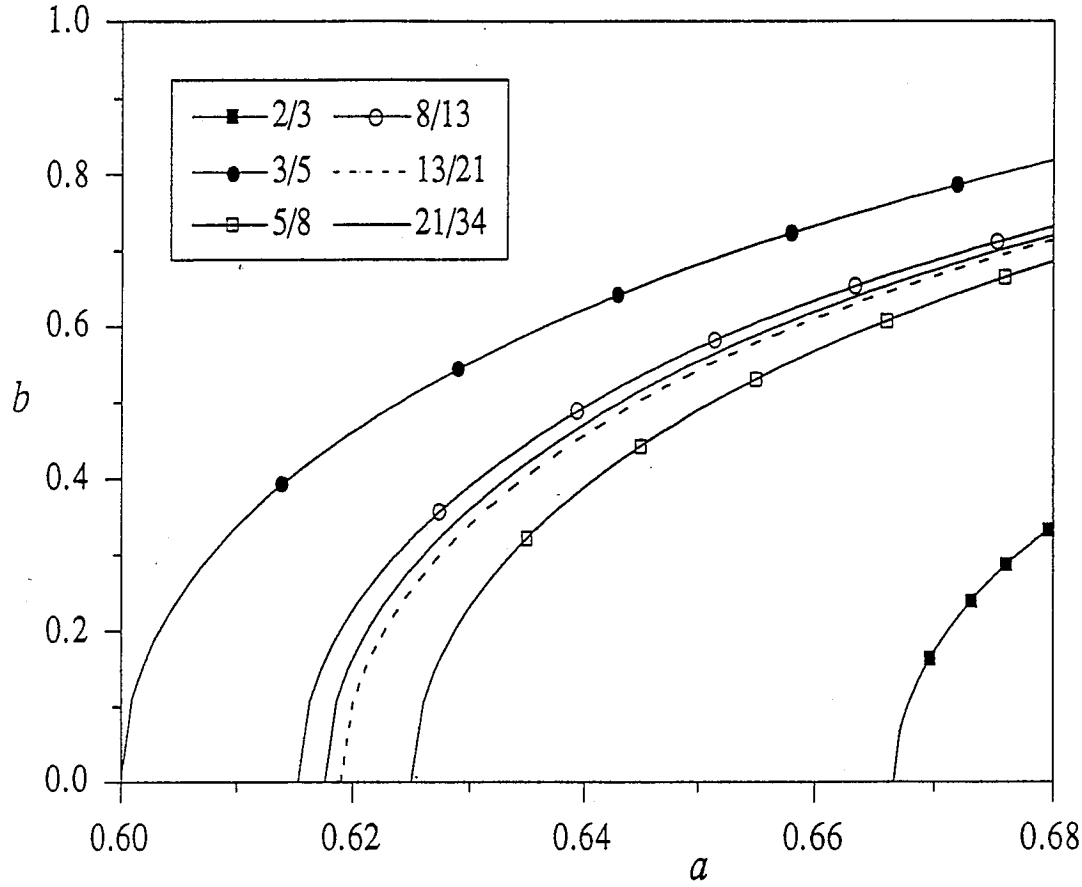

FIGURE 4

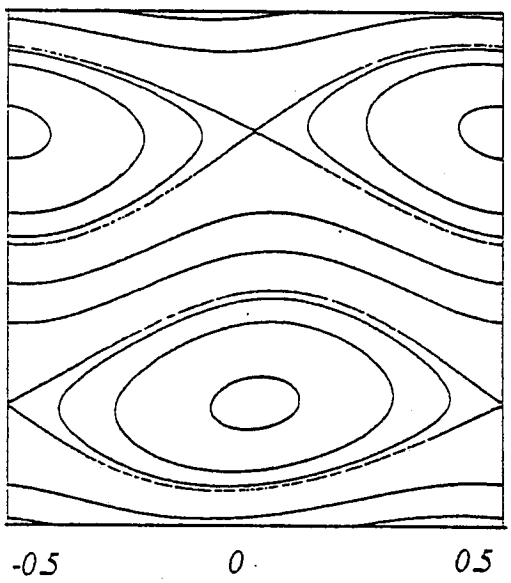

(a)

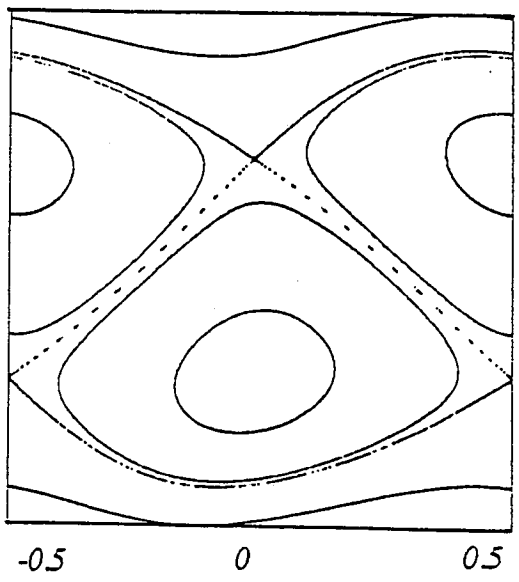

(b)

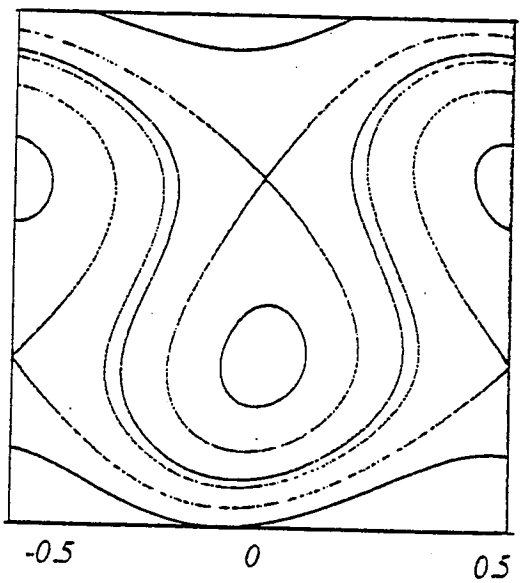

(c)

FIGURE 5

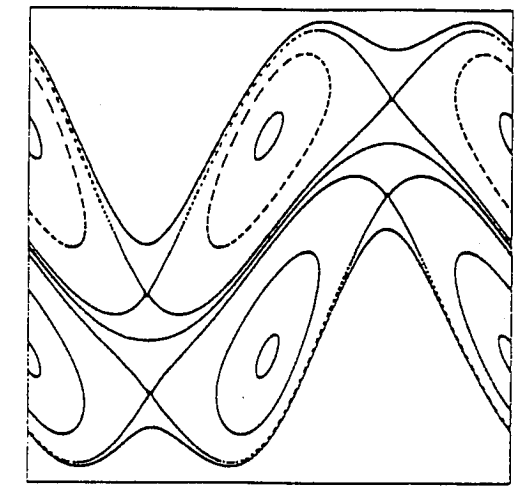

(a)

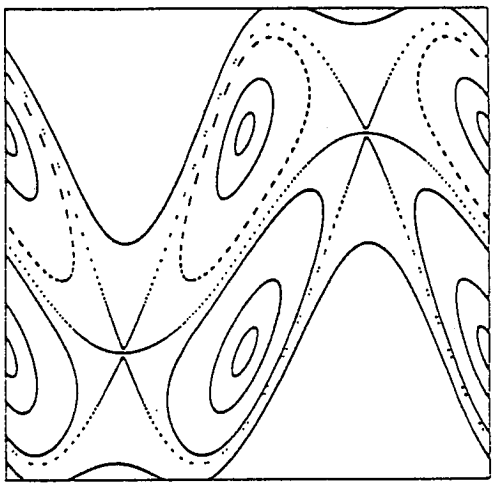

(b)

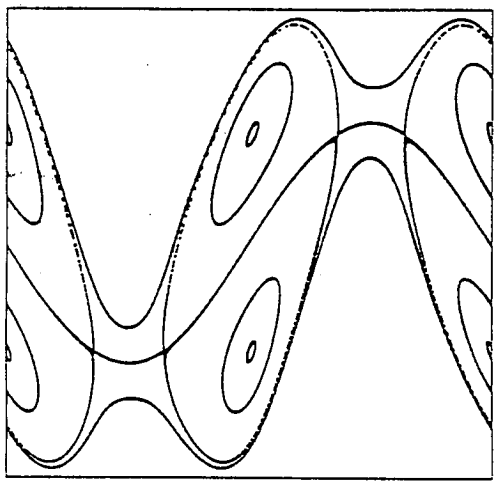

(c)

FIGURE 6

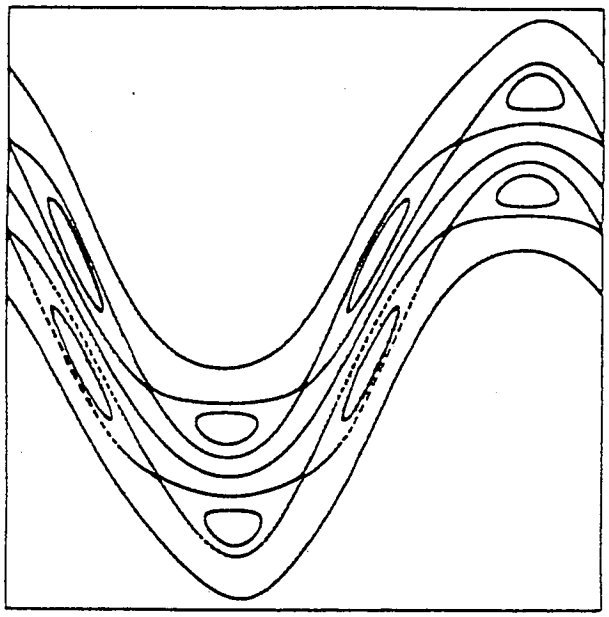

(a)

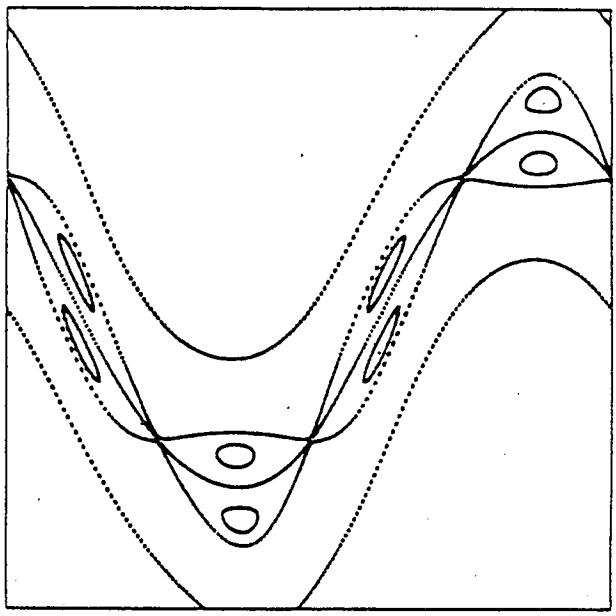

(b)

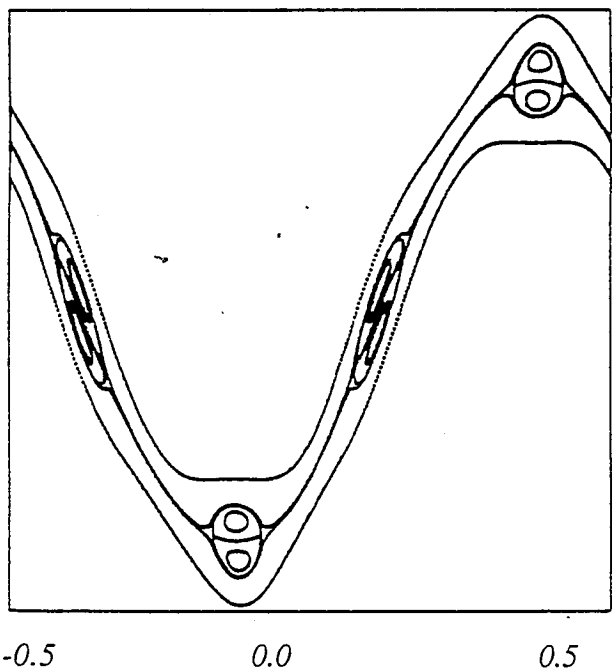

(c)

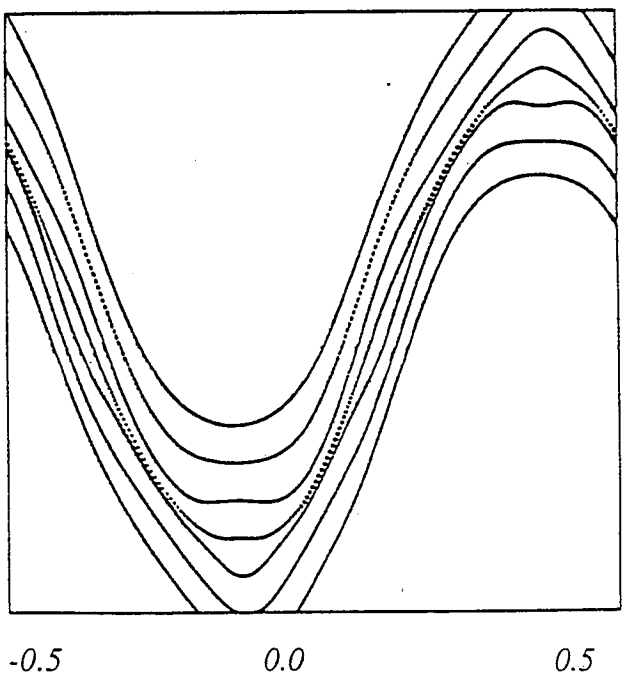

(d)

FIGURE 7

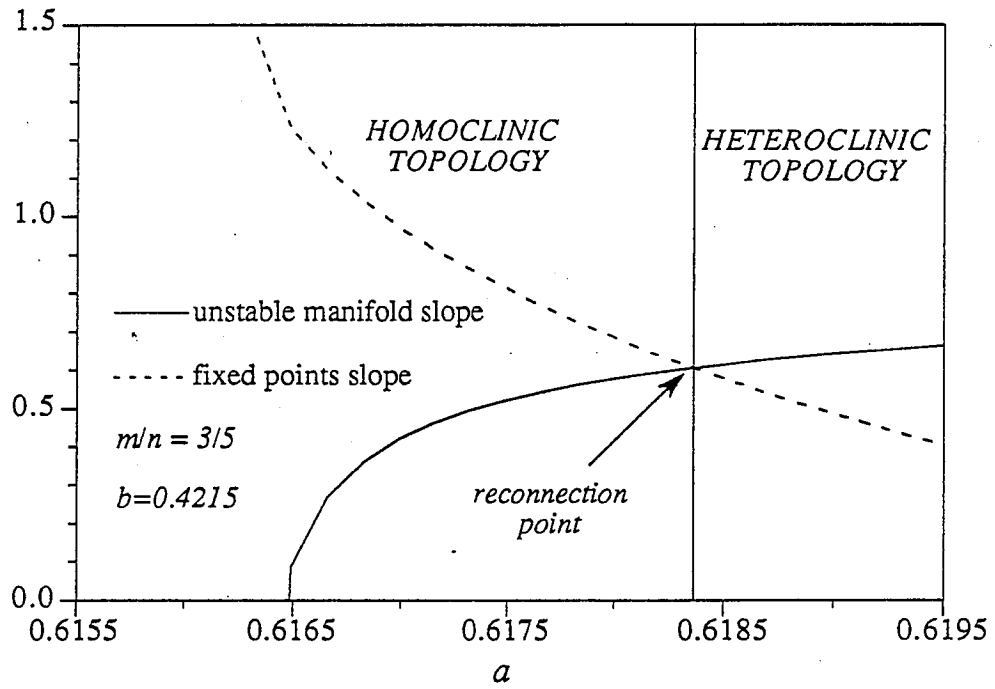
1.5
1.0
0.5
0.0
HOMOCLINIC
TOPOLOGY
HETEROCLINIC
TOPOLOGY
unstable manifold slope
fixed points slope
m/n = 3/5
b=0.4215
reconnection
point
0.6155
0.6165
0.6175
0.6185
0.6195
a

FIGURE 8

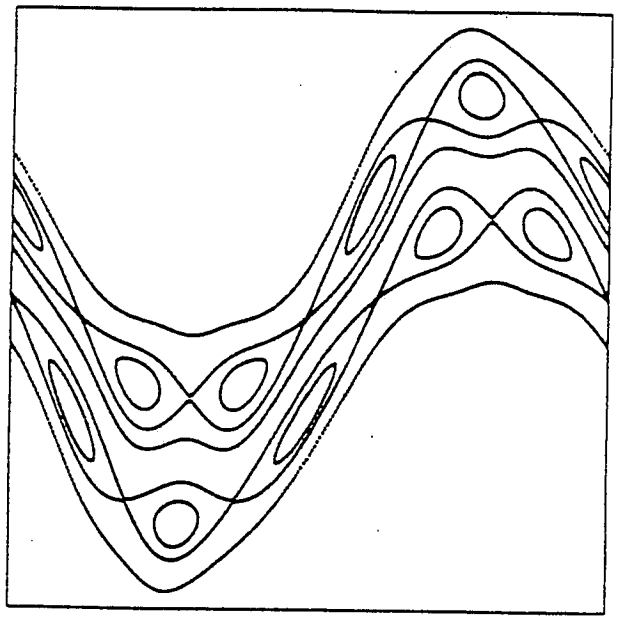

(a)

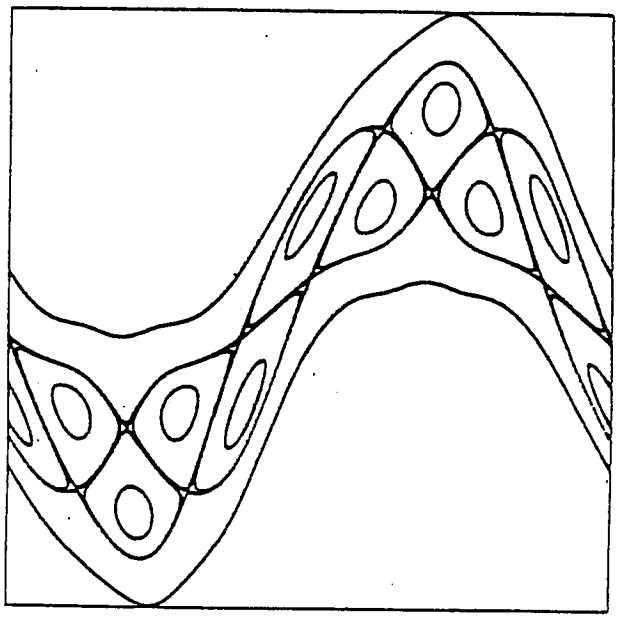

(b)

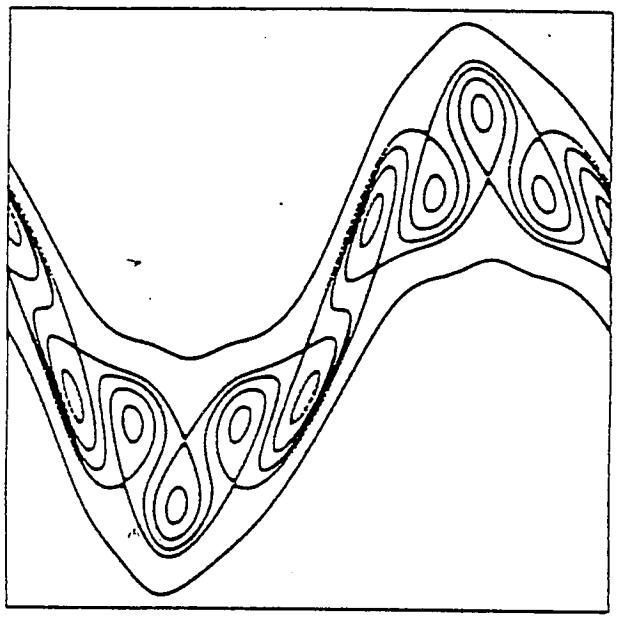

(c)

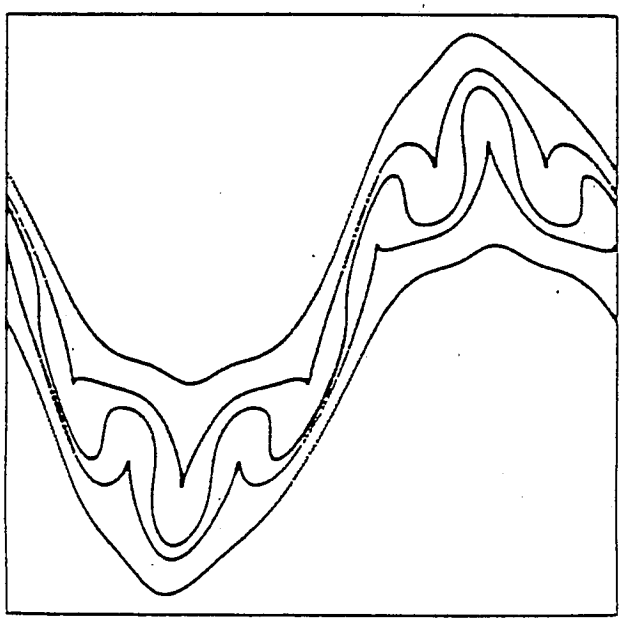

(d)

FIGURE 9

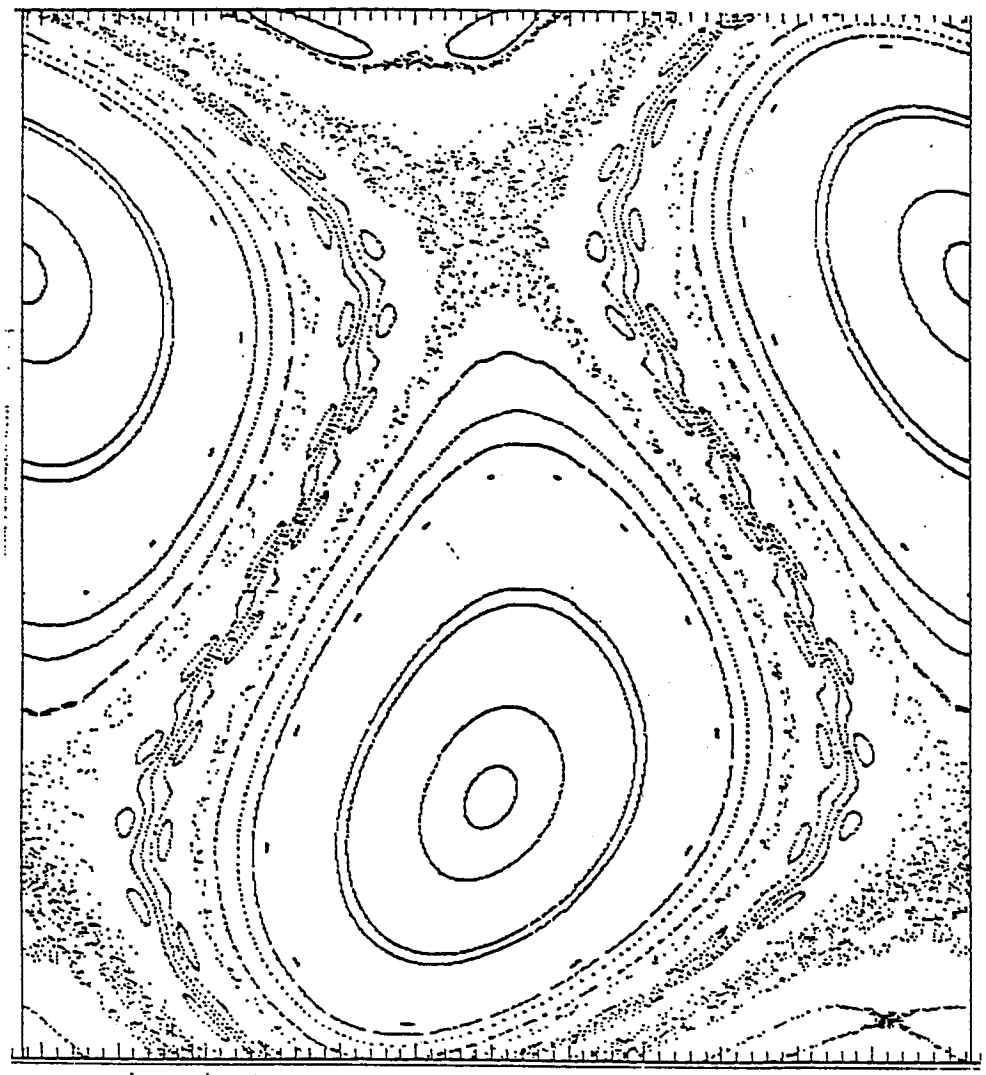

FIGURE 10

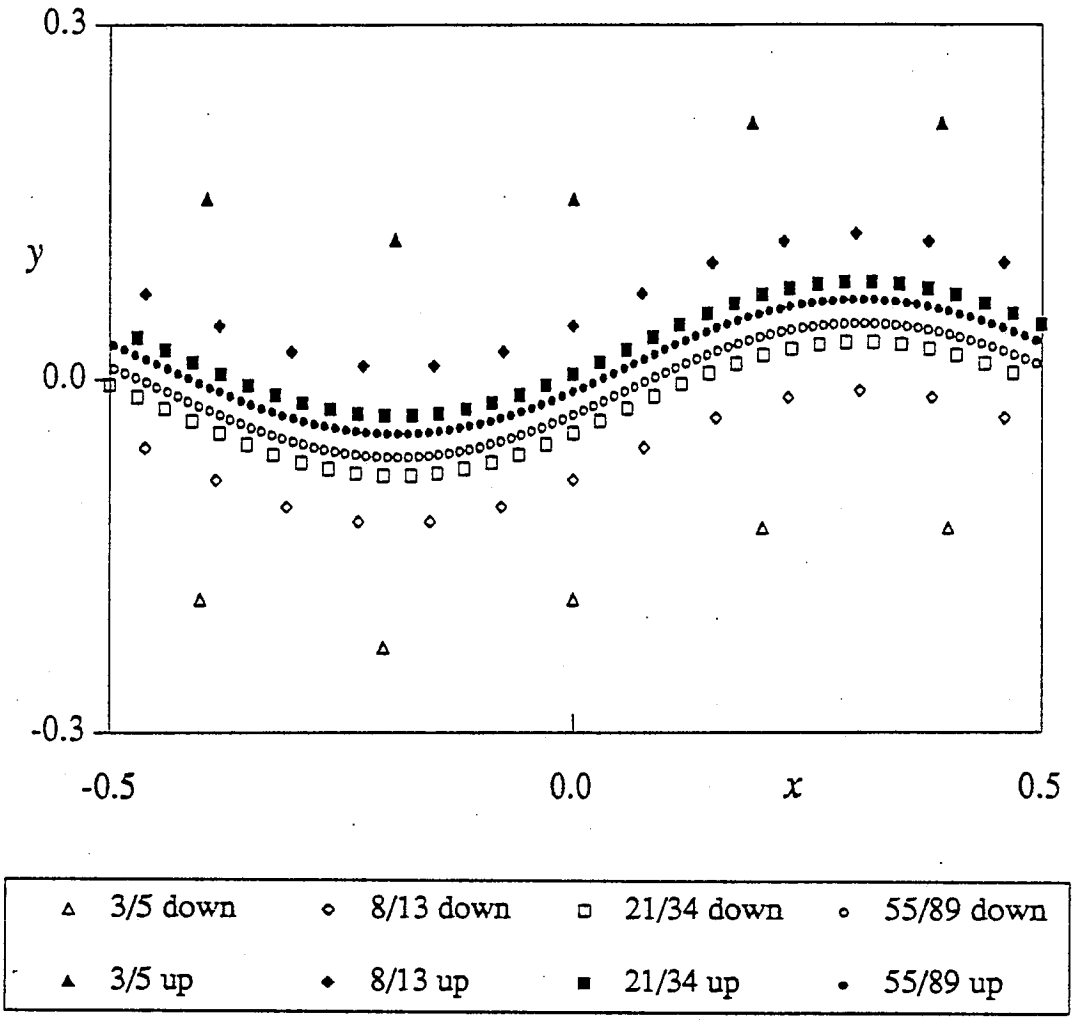
0.3
y
0.0
-0.3
-0.5
0.0
x
0.5
3/5 down
8/13 down
21/34 down
55/89 down
3/5 up
8/13 up
21/34 up
55/89 up

FIGURE 11

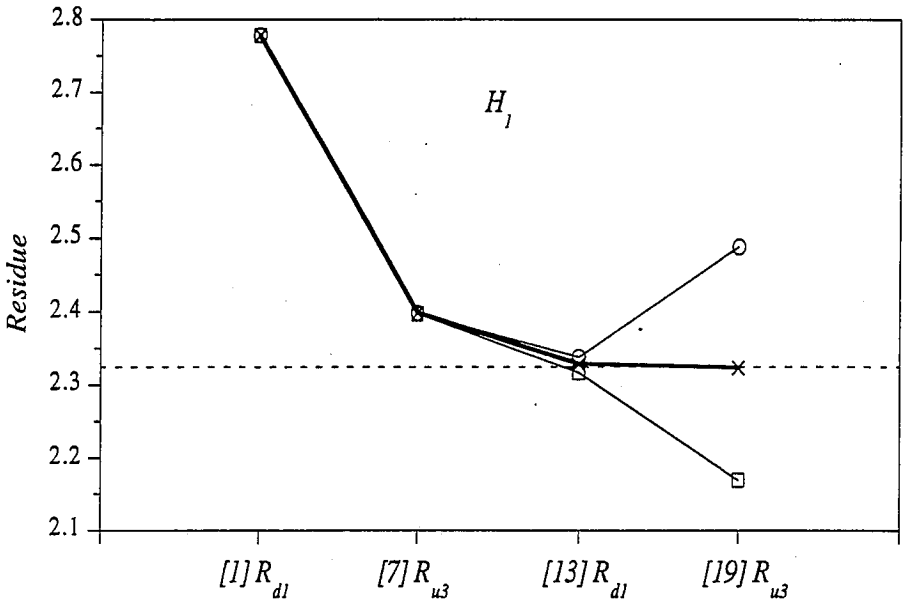
2.8
2.7
2.6
2.5
2.4
2.3
2.2
2.1
Residue
H_1
[1] R_{d1}
[7] R_{u3}
[13] R_{d1}
[19] R_{u3}

(a)

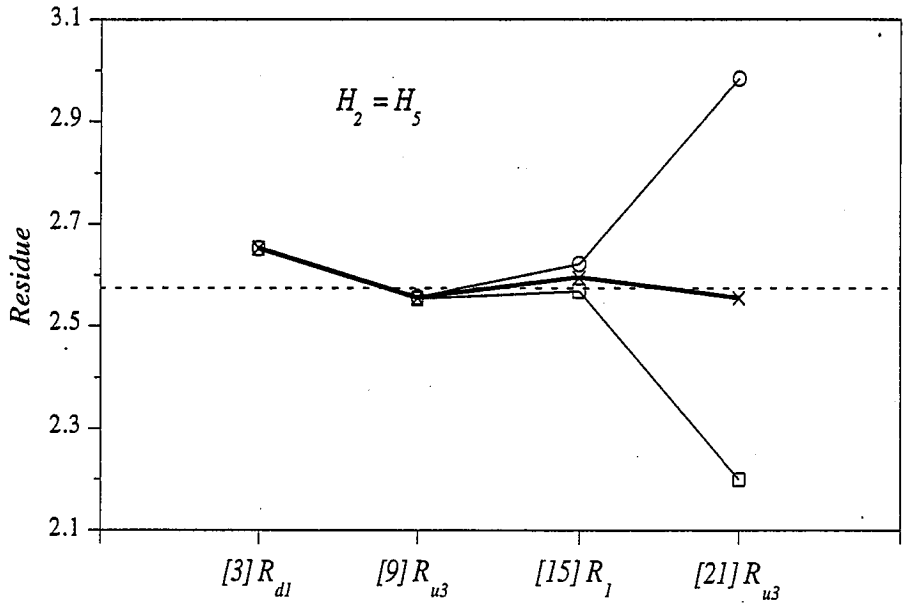
3.1
2.9
2.7
2.5
2.3
2.1
Residue
$H_2 = H_5$
[3] R_{d1}
[9] R_{u3}
[15] R_1
[21] R_{u3}

(b)

FIGURE 12

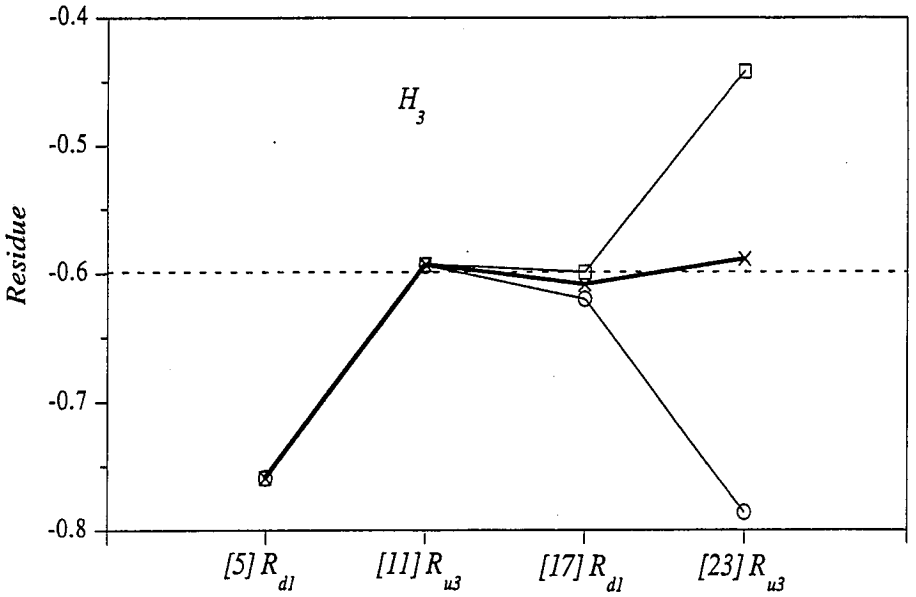
-0.4
-0.5
-0.6
-0.7
-0.8
Residue
H_3
[5] R_{d1}
[11] R_{u3}
[17] R_{d1}
[23] R_{u3}

(c)

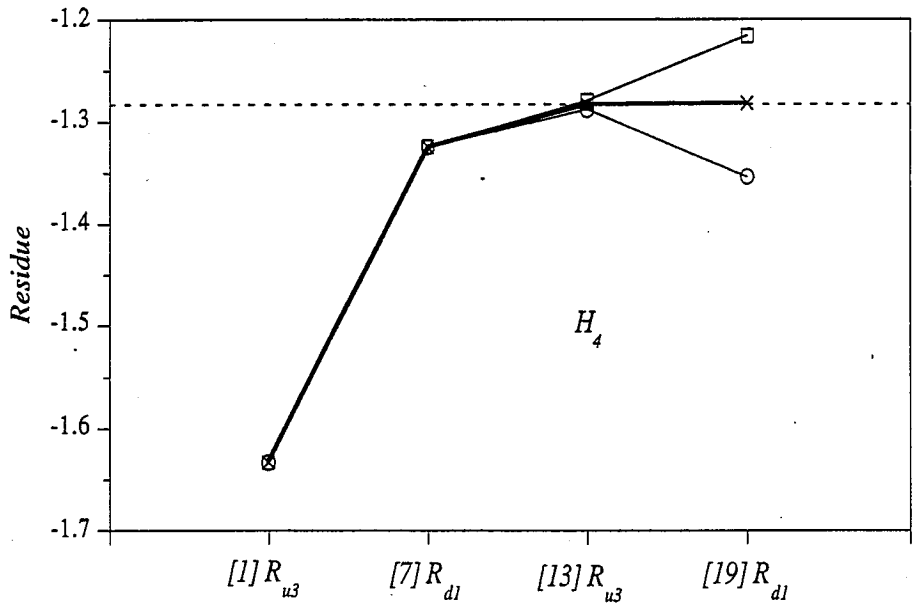
-1.2
-1.3
-1.4
-1.5
-1.6
-1.7
Residue
H_4
[1] R_{u3}
[7] R_{d1}
[13] R_{u3}
[19] R_{d1}

(d)

FIGURE 12

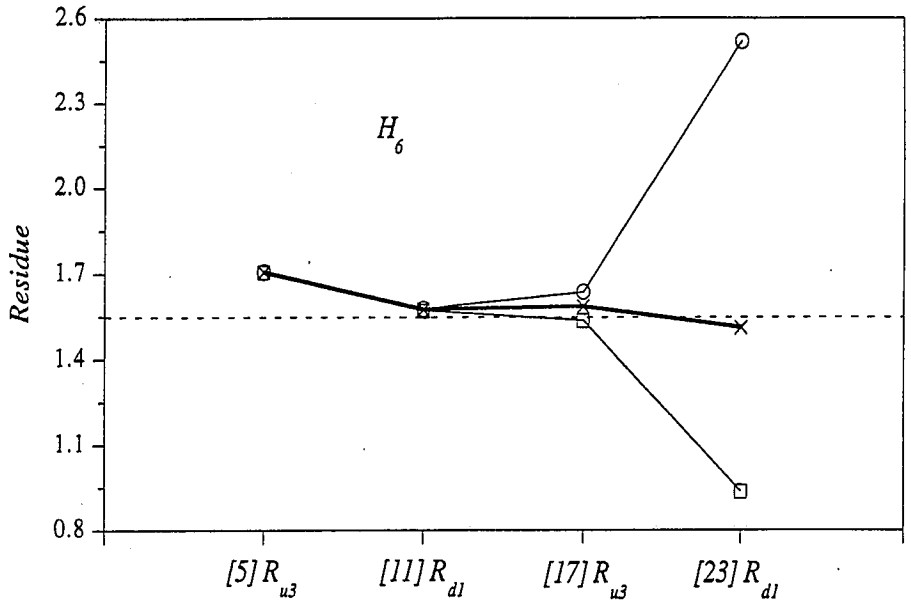

(e)

FIGURE 12

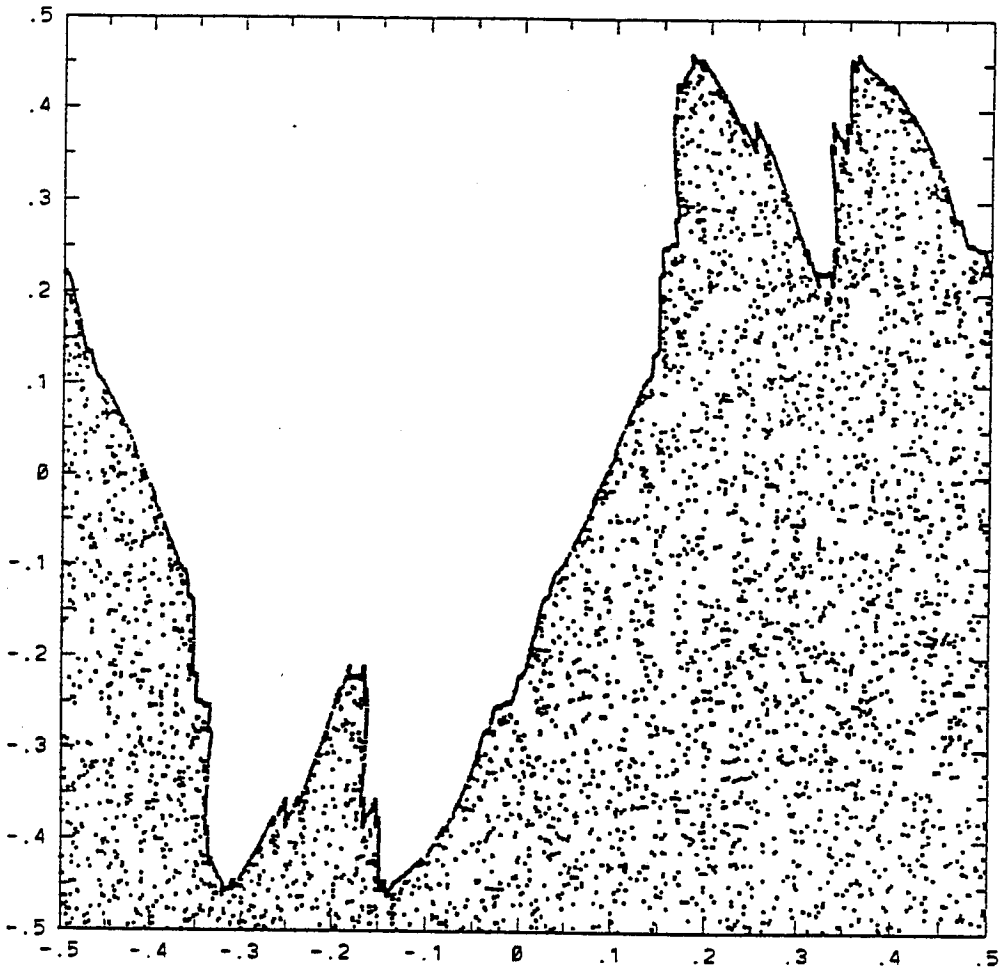

FIGURE 13

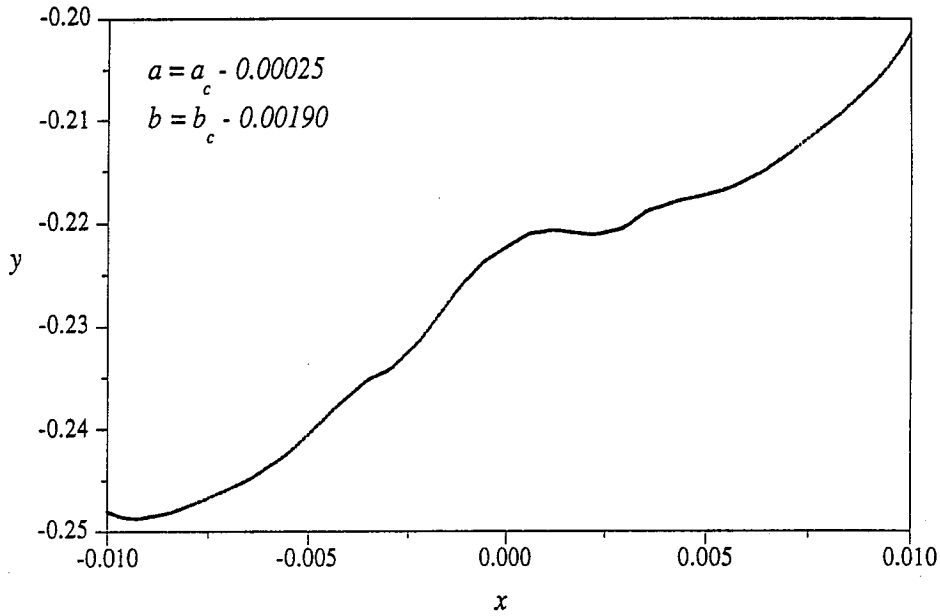
-0.20
-0.21
-0.22
-0.23
-0.24
-0.25
y
a = a_c - 0.00025
b = b_c - 0.00190
-0.010
-0.005
0.000
0.005
0.010
x

(a)

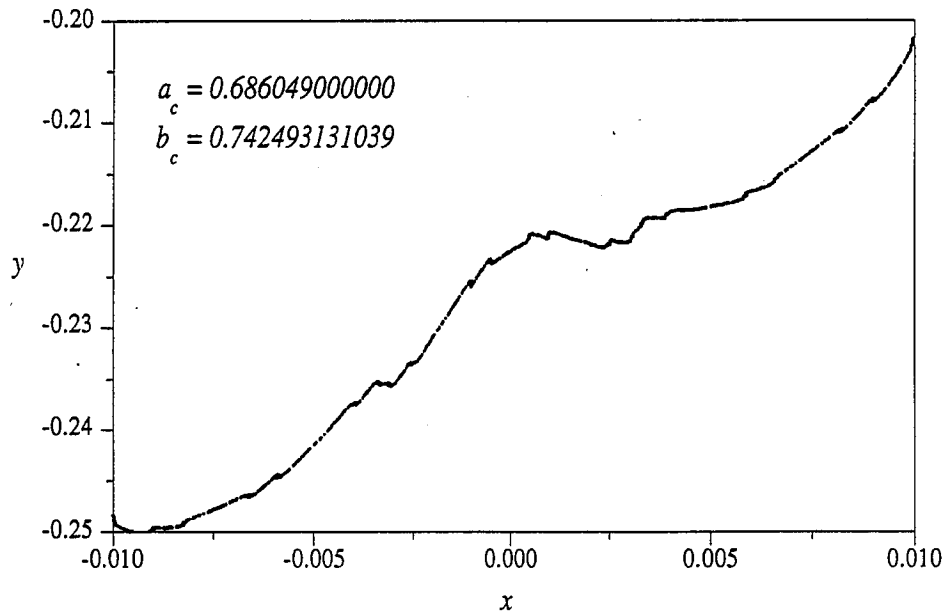
-0.20
-0.21
-0.22
-0.23
-0.24
-0.25
y
a_c = 0.686049000000
b_c = 0.742493131039
-0.010
-0.005
0.000
0.005
0.010
x

(b)

FIGURE 14

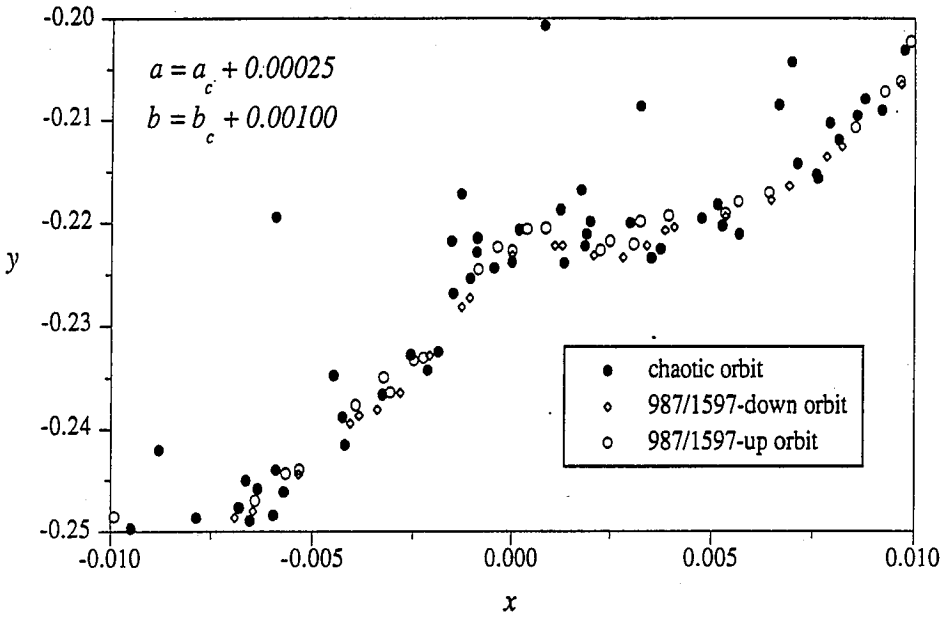
-0.20
-0.21
-0.22
-0.23
-0.24
-0.25
y
$a = a_c + 0.00025$
$b = b_c + 0.00100$
chaotic orbit
987/1597-down orbit
987/1597-up orbit
-0.010
-0.005
0.000
0.005
0.010
x

(c)

FIGURE 14

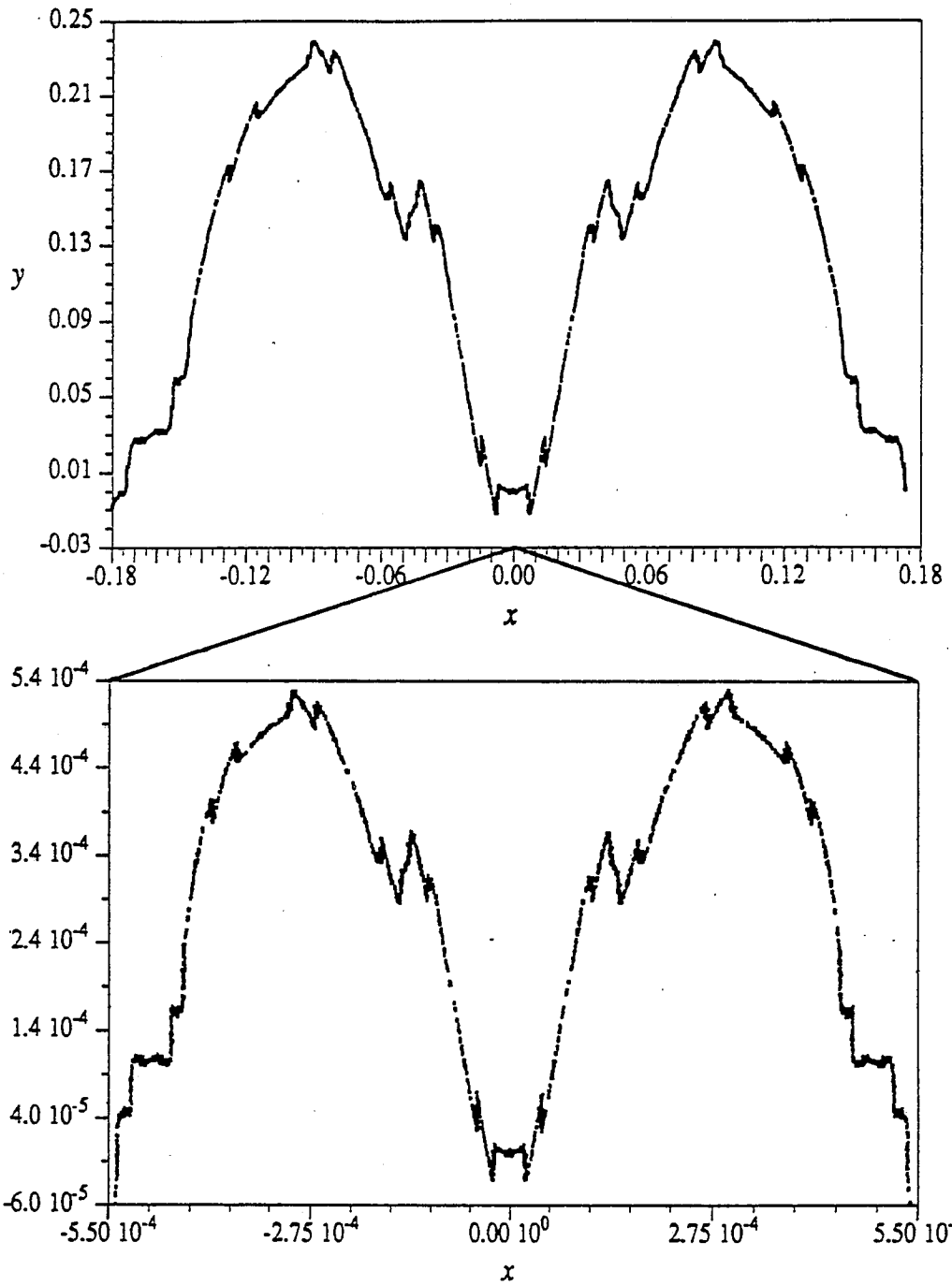
0.25
0.21
0.17
0.13
y
0.09
0.05
0.01
-0.03
-0.18
-0.12
-0.06
0.00
0.06
0.12
0.18
x
(a)
5.4 10-4
4.4 10-4
3.4 10-4
2.4 10-4
1.4 10-4
4.0 10-5
-6.0 10-5
-5.50 10-4
-2.75 10-4
0.00 100
2.75 10-4
5.50 10-4
x
(b)

FIGURE 15